Supplementary Information

Critical Role of H-Aggregation for High-Efficiency Photoinduced Charge Generation in Pristine Pentamethine Cyanine Salts

George C. Fish,[a] Juan Manuel Moreno-Naranjo,[a†] Andreas Billion,[b] Daniel Kratzert,[b] Erwin Hack,[c] Ingo Krossing,[b] Frank Nüesch[d,e] and Jacques-E. Moser*[a]

a) *Photochemical Dynamics Group, Institute of Chemical Sciences and Engineering, École polytechnique fédérale de Lausanne, Station 6, 1015 Lausanne, Switzerland.*

b) *Institut für Anorganische und Analytische Chemie, and Freiburger Materialforschungszentrum, Universität Freiburg, Albertstrasse 21, 79104 Freiburg, Germany.*

c) *Laboratory for Transport at Nanoscale Interfaces, Swiss Federal Laboratories for Materials Science and Technology, Empa, Überlandstrasse 129, 8600 Dübendorf, Switzerland.*

d) *Laboratory for Functional Polymers, Swiss Federal Laboratories for Materials Science and Technology, Empa, Überlandstrasse 129, 8600 Dübendorf, Switzerland.*

e) *Institute of Materials, School of Engineering, École polytechnique fédérale de Lausanne, Station 12, 1015 Lausanne, Switzerland.*

† Current address: Department of Chemistry, Molecular Sciences Research Hub, Imperial College London, White City Campus, London, W12 OBZ, United Kingdom

* *Corresponding author. Email: je.moser@epfl.ch*

S1. Synthetic Procedure for the preparation of Cy5-[Al(pftb)$_4$] and Cy5-[Al(pfad)$_4$]

General Working Technique

All manipulations were carried out under an inert argon atmosphere, using standard vacuum and Schlenk techniques with a pressure of 10^{-3} mbar or a glove box (MBraun Lab Master) with argon atmosphere and H_2O and O_2 contents <1 ppm to exclude air and moisture. All solvents and reagents were dried using conventional drying agents, distilled afterwards and stored under argon atmosphere over activated 3 Å molecular sieves.

NMR Spectroscopic Investigations

NMR samples were prepared in an inert atmosphere glove box in NMR tubes equipped with a gas-tight J. Young valve. NMR spectra were recorded on a Bruker Avance II$^+$ 400 MHz WB and a Bruker Avance III HD 300 MHz NMR spectrometer at room temperature (unless described otherwise) using the software package Bruker TopSpin 4.0.7 for analysis. The spectra were calibrated based on the chemical shift of the deuterated solvents used.

Single Crystal X-ray Diffraction

The data was collected from shock-cooled single crystals at 100(2) K on a Bruker D8 VENTURE dual wavelength Mo/Cu three-circle diffractometer with a microfocus sealed X-ray tube using mirror optics as monochromator and a Bruker PHOTON III detector. The diffractometer was equipped with an Oxford Cryostream 800 low temperature device and used MoK_α radiation (λ = 0.71073 Å). All data were integrated with SAINT and a multi-scan absorption correction using SADABS was applied.[1,2] The structure were solved by direct methods using SHELXT and refined by full-matrix least-squares methods against F^2 by SHELXL-2018/3.[3,4] All non-hydrogen atoms were refined with anisotropic displacement parameters. The hydrogen atoms were refined isotropically on calculated positions using a riding model with their U_{iso} values constrained to 1.5 times the U_{eq} of their pivot atoms for terminal sp^3 carbon atoms and 1.2 times for all other carbon atoms. Crystallographic data for the structures reported in this paper have been deposited with the Cambridge Crystallographic Data Centre.[5] CCDC 2044614 and 2056417 contain the supplementary crystallographic data for this paper. These data can be obtained free of charge from The Cambridge Crystallographic Data Centre via www.ccdc.cam.ac.uk/structures. This report and the CIF file were generated using FinalCif.[6]

S1.1 Synthesis and Characterization of the [Cy5][Al(pftb)$_4$] (pftb = OC(CF$_3$)$_3$)

Li[Al(OC(CF$_3$)$_3$)$_4$] (1.092 g, 1.121 mmol) and [Cy5][BF$_4$] (0.521 g, 1.108 mmol, 1.00 eq) were submitted into a H-cell equipped with a G4 frit and dissolved in CH$_2$Cl$_2$ (10 mL) and stirred at r.t. for 3 days. The reaction mixture was sonicated for 1 h and filtered after the precipitation of solid could be observed. The solvent was removed under reduced pressure und the title compound was isolated as blue powder (1.23 g, 0.911 mmol, 82 %) and characterized by NMR spectroscopy.

Recorded NMR spectra of [Cy5][Al(OC(CF$_3$)$_3$)$_4$] in CD$_2$Cl$_2$, CDCl$_3$ and o-DFB always showed heavily broadened resonances in the ^{1}H-NMR spectra in contrast to the reference spectrum of [Cy5][BF$_4$] (Figure S1.1). These broadened resonances in the regions of 2.37 to 4.80 and 5.80 to 8.50 ppm show no clear splitting pattern but are the main resonances and caused by [Cy5][Al(OC(CF$_3$)$_3$)$_4$]. A precise assignment of the resonances of the title compound is not possible due to the enlargement with exception of the intensive singlet at 1.71 ppm caused by the CH$_3$ groups (H8)) of [Cy5][Al(OC(CF$_3$)$_3$)$_4$]. The ^{1}H-NMR spectrum further shows

resonances, which can be assigned to indoline moieties (Ind1, In2, **Erreur ! Source du renvoi introuvable.**S1.2) which indicate a partial decomposition of the cation [Cy5] but only represent 1 % of the intensity in the NMR sample. The assignment of the resonances of the decomposition products were completed, considering the ^{1}H,^{13}C-HSQC and ^{1}H,^{13}HMBC NMR spectra in Figures S1.3 and S1.4. The complete assignment is summarized in Table S1.1 and visualized in Figure S1.2.

Starting material [Cy5][BF$_4$] – reference NMR spectrum
^{1}H-NMR (400.17 MHz, 298 K, CDCl₃): δ = 1.68 (s, 12H, H(8)), 3.59 (s, 6H, H(13)), 6.15 (d, $^3J_{H,H}$ = 13.5 Hz, 2H, H(10)), 6.61 (t, $^3J_{H,H}$ = 12.5 Hz, 1H, H(12), 7.11 (d, $^3J_{H,H}$ = 8.1 Hz, 2H, H(2)), 7.18 (t, $^3J_{H,H}$ = 7.5 Hz, 2H, H(4)), 7.33 (m, 4H, H(5), H(3)), 8.02 (dd, $^3J_{H,H}$ = 13.3 Hz, 2H, H(11)) ppm.
^{11}B-NMR (128.39 MHz, 298 K, CDCl₃): δ = −0.7 (br. s, 1B, **B**F$_4$) ppm.
^{13}C-NMR (100.62 MHz, 298 K, CDCl₃): δ = 27.8 (C8), 31.4 (C13), 49.6 (C7), 103.6 (C10), 110.5 (C2), 122.2 (C5), 125.1 (C12), 126.0 (C4), 128.7 (C3), 141.3 (C6), 142.8 (C1), 154.1 (C11), 173.7 (C9) ppm.
^{19}F-NMR (376.54 MHz, 298 K, CDCl₃): δ = −152.0 (q, $^2J_{F,B}$ = 0.9 Hz, B^{11}**F**, 4F, [BF$_4$]$^-$), −151.9 (m, B^{10}**F**, 4F, [BF$_4$]$^-$) ppm.

[Cy5][Al(OC(CF$_3$)$_3$)$_4$]
^{1}H-NMR (400.17 MHz, 298 K, CDCl₃): δ = 1.68 (s, 6H, H(8)-Ind1), 1.71 (s, 12H, H(8)), 1,72(s, 6H, H(8)-Ind2), 2.37-4.80 (very broadened resonance, 6H, H(13)), 4.01 (br. s, 3H, H(10)-Ind2), 4.07 (br. s, 3H, H(10)-Ind1), 5.80-8.50 (very broadened resonance, 13H, H(10), H(12), H(2), H(4), H(5), H(3), H(11) ppm.
^{13}C-NMR (100.62 MHz, 298 K, CDCl₃): δ = 21.9 (C8-Ind1), 25.6 (C8-Ind2), 34.3 (C10-Ind2), 35.2 (C10-Ind1), 53.4 (C7-Ind1), 53.6 (C7-Ind2), 140.6 (C1-Ind2), 140.9 (C1-Ind1), 141.0 (C6-Ind1), 143.0 (C6-Ind2), 181.9 (C9-Ind2), 192.4 (C9-Ind1) ppm.
^{19}F-NMR (376.54 MHz, 298 K, CDCl₃): δ = −75.7 (s, 36F, [Al(OC(C**F$_3$**)$_3$)$_4$]$^-$) ppm.
^{27}Al-NMR (104.27 MHz, 298 K, CDCl₃): δ = 34.6 (s, 1Al, [**Al**(OC(CF$_3$)$_3$)$_4$]$^-$) ppm.
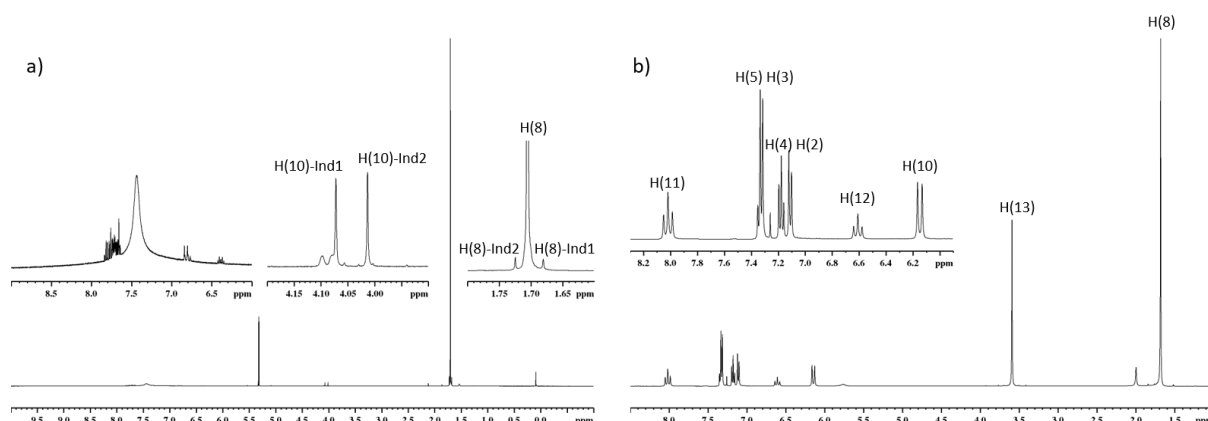
Figure S1.1. a) ^{1}H-NMR spectrum (400.17 MHz, 298 K, CDCl$_3$) Synthesis of [Cy5][Al(OC(CF$_3$)$_3$)$_4$] showing very small impurities by indoline species. b) ^{1}H-NMR spectrum (400.17 MHz, 298 K, CDCl$_3$) Reference spectrum of [Cy5][BF$_4$].

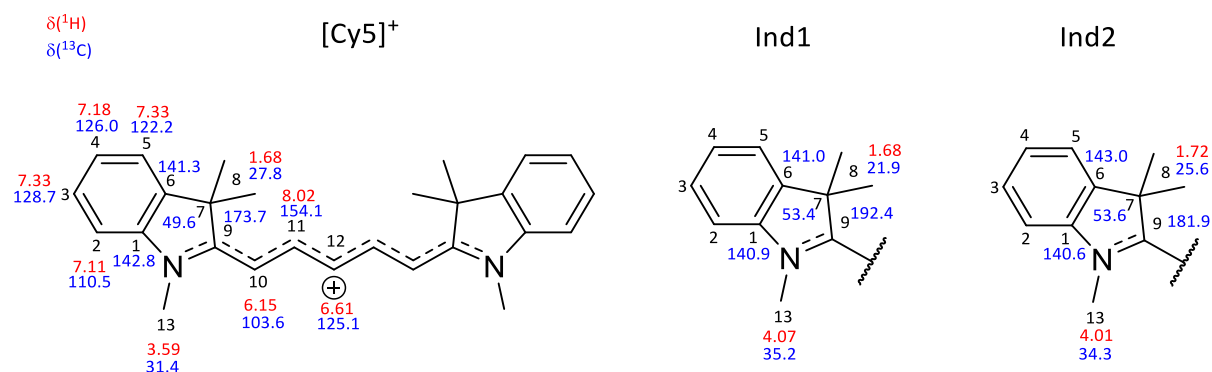**Figure S1.2.** Assignment of the ^{1}H and ^{13}C chemical shifts of [Cy5][BF$_4$], Ind1 and In2.

Table S1.1. Overview of the ^{1}H and ^{13}C chemical shifts of [Cy5][BF$_4$], Ind1 and Ind2.

Position	[Cy5][BF$_4$] $\delta(^1H)$	$\delta(^{13}C)$	Ind1 $\delta(^1H)$	$\delta(^{13}C)$	Ind2 $\delta(^1H)$	$\delta(^{13}C)$
1		142.8		140.9		140.6
2	7.11	110.5				
3	7.33	128.7				
4	7.18	126.0				
5	7.33	122.2				
6		141.3		141.0		143.0
7		49.6		53.4		53.6
8	1.68	27.8	1.68	21.9	1.72	25.6
9		173.7		192.4		181.9
10	6.15	103.6				
11	8.02	154.1				
12	6.61	125.1				
13	3.59	31.4	4.07	35.2	4.01	34.3
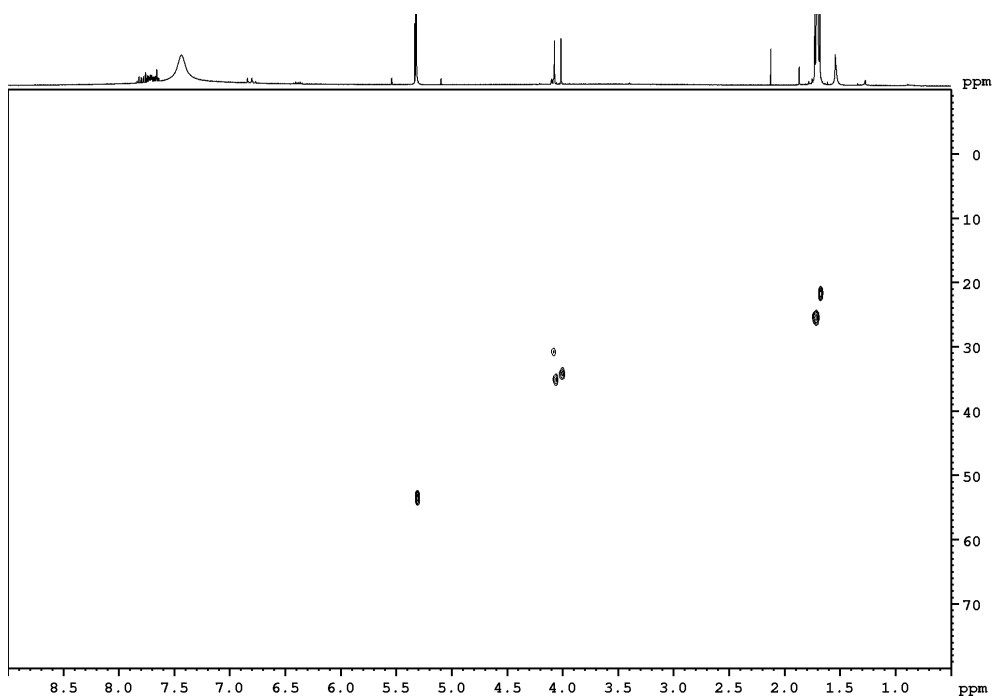
Figure S1.3. ^{1}H,^{13}C-HSQC NMR spectrum (400.17 MHz, optimized on 1 Hz, 298 K, CD$_2$Cl$_2$) of the synthesis of [Cy5][Al(OC(CF$_3$)$_3$)$_4$].
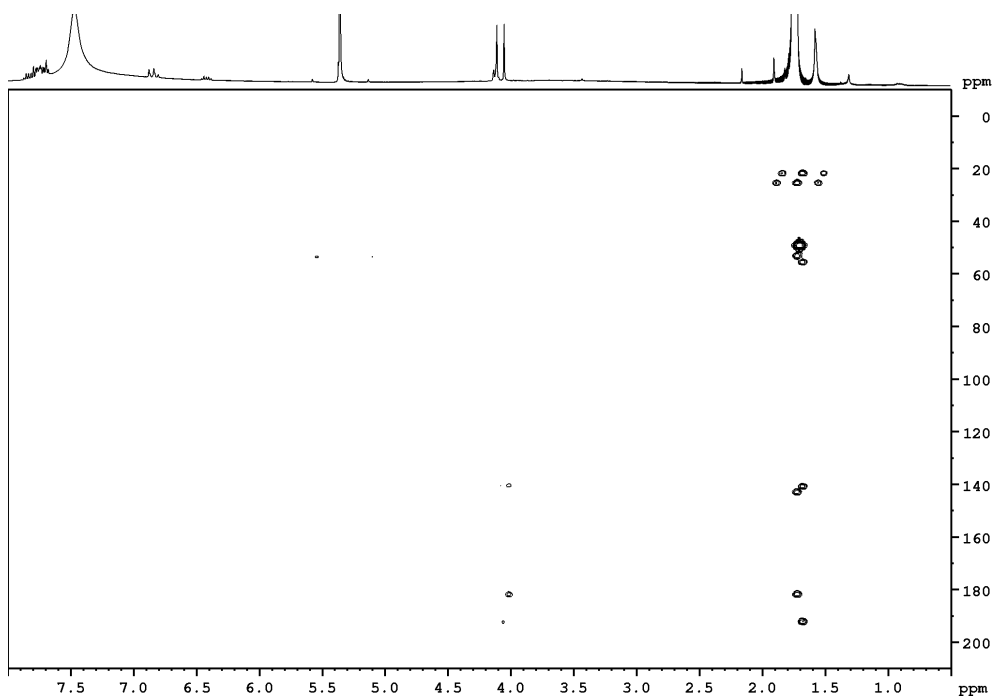
Figure S1.4. ^{1}H,^{13}C-HMBC NMR spectrum (400.17 MHz, optimized on 8 Hz, 298 K, CD$_2$Cl$_2$) of the synthesis of [Cy5][Al(OC(CF$_3$)$_3$)$_4$].
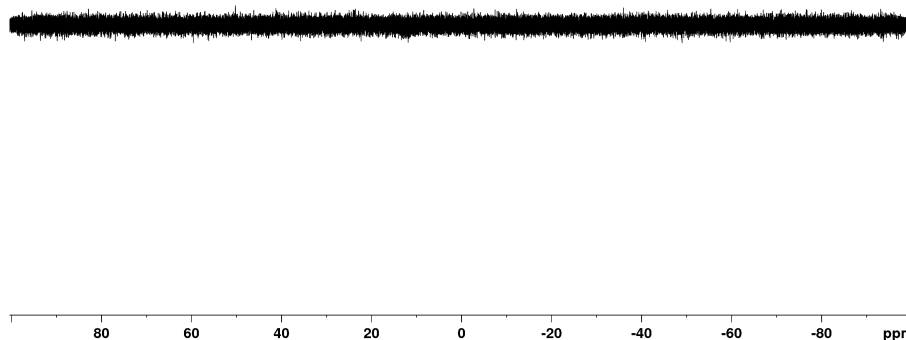
Figure S1.5. ^{7}Li-NMR spectrum (155.52 MHz, 298 K, CDCl$_3$) of the synthesis of [Cy5][Al(OC(CF$_3$)$_3$)$_4$]. Li$^+$ is absent.
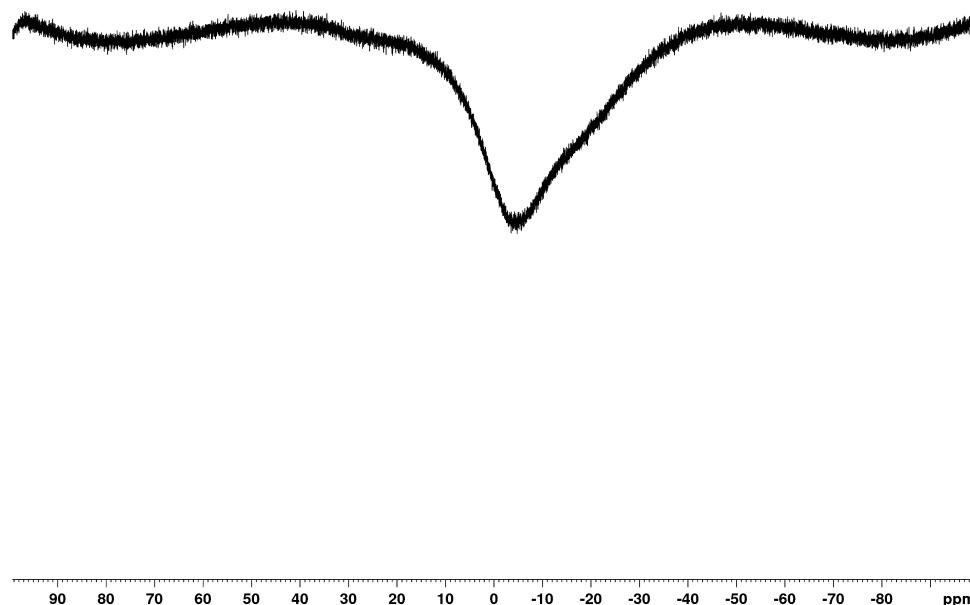
Figure S1.6. ^{11}B-NMR spectrum (128.39 MHz, 298 K, CDCl$_3$) of the synthesis of [Cy5][Al(OC(CF$_3$)$_3$)$_4$]. BF$_4^-$ is absent.
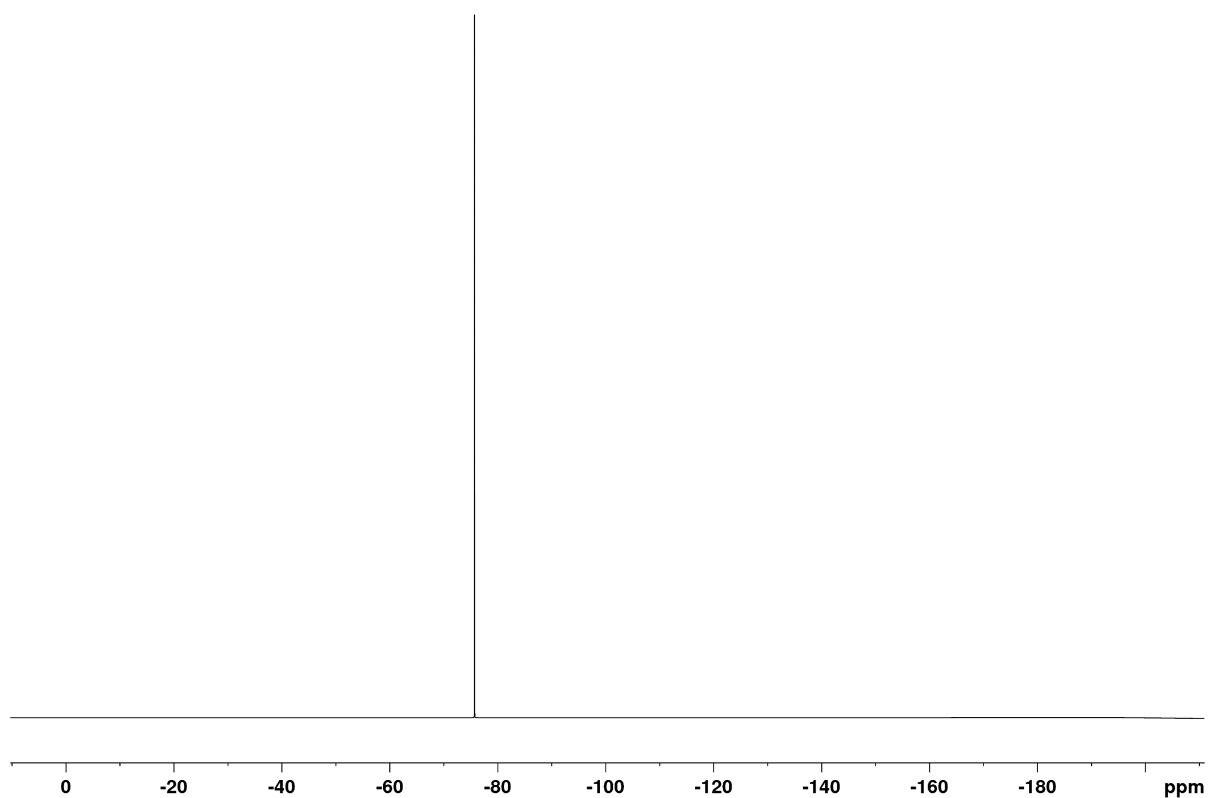
Figure S1.7. ^{19}F-NMR spectrum (376.54 MHz, 298 K, CDCl$_3$) of the synthesis of [Cy5][Al(OC(CF$_3$)$_3$)$_4$].
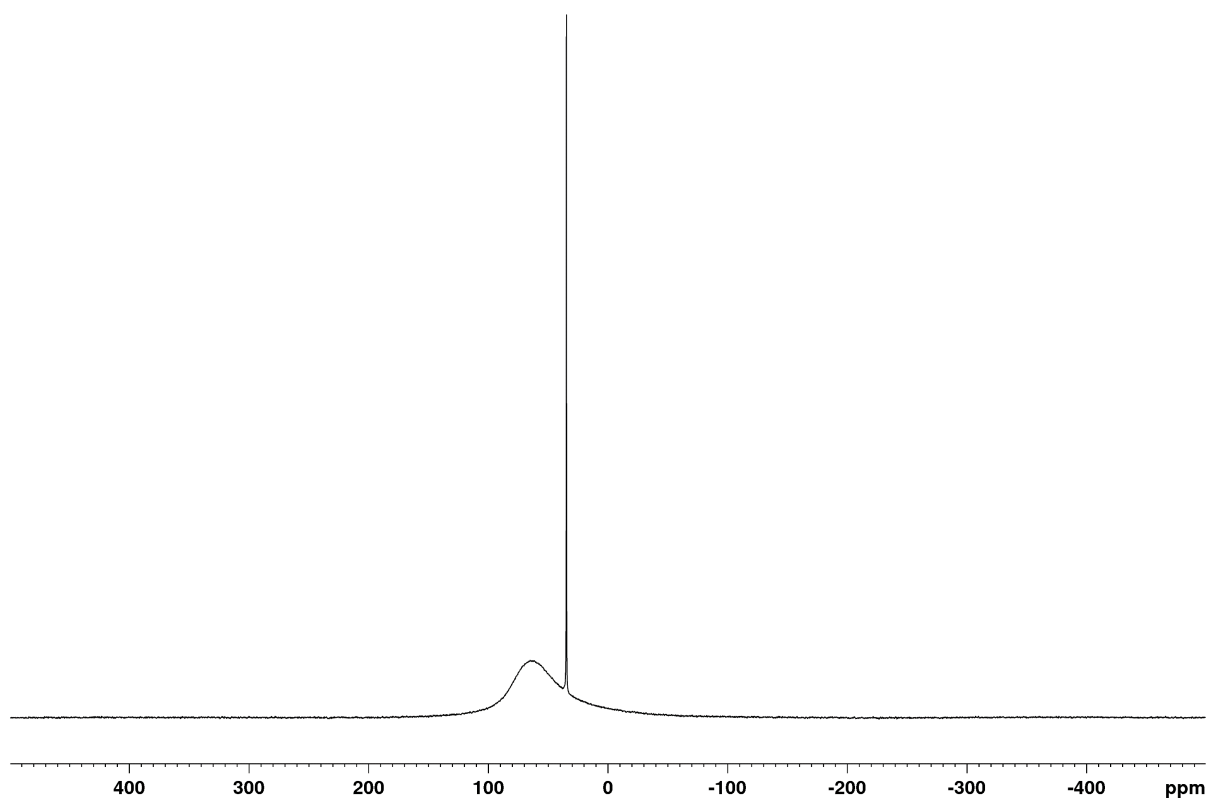
Figure S1.8. ^{27}Al-NMR spectrum (104.27 MHz, 298 K, CDCl$_3$) of the synthesis of [Cy5][Al(OC(CF$_3$)$_3$)$_4$].

S1.2. Synthesis and Characterization of the [Cy5][Al(pfad)$_4$] (pfad = perfluoroadamantoxy = OC$_{10}$F$_{15}$)

Li[Al(OC$_{10}$F$_{15}$)$_4$] (0.650 g, 0.378 mmol) and [Cy5][BF$_4$] (0.181 g, 0.385 mmol, 1.02 eq) were submitted into a H-cell equipped with a G4 frit und dissolved in CH$_2$Cl$_2$ (10 mL) and stirred for 2 days at r.t. The reaction mixture was sonicated for 20 h and filtered after the precipitation of solid could be observed. The solvent was removed under reduced pressure und the title compound was isolated as green powder. NMR investigations showed impurities by C$_{10}$F$_{15}$OH/C$_{10}$F$_{15}$O$^-$. The obtained solid was dissolved in CH$_2$Cl$_2$ (10 mL) and suitable crystals for single crystal XRD experiments were obtained by slow vapor diffusion with *n*-pentane. After single crystal XRD experiments were done, the reaction solution was filtered, the crystalline residue washed with *n*-pentane (2x 4.0 mL) and dried in *vacuo*. The pure target compound was isolated as a yellow gleaming solid (0.20 g, 0.095 mmol, 25.0 %) and characterized by NMR spectroscopy.
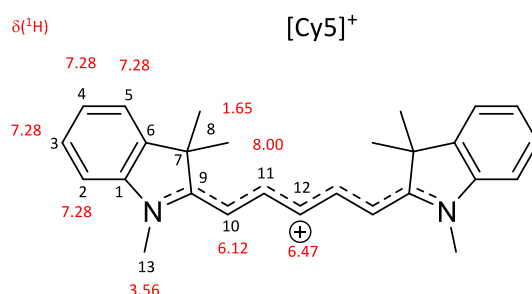
^{1}H-NMR (300.18 MHz, 298 K, THF/CDCl$_3$): δ = 1.65 (s, 12H, H(8)), 3.56 (s, 6H, H(13)), 6.12 (d, $^3J_{H,H}$ = 13.8 Hz, 2H, H(10)), 6.47 (t, $^3J_{H,H}$ = 12.5 Hz, 1H, H(12), 7.28 (m, 8H, H(2), H(4) H(5), H(3)), 8.00 (dd, $^3J_{H,H}$ = 13.0 Hz, 2H, H(11)) ppm.

^{19}F-NMR (282.45 MHz, 298 K, THF/CDCl$_3$): δ = −223.7 (s, C**F**, 12F, [Al(OC$_{10}$F$_{15}$)$_4$]$^-$), −122.0 (m, C**F$_2$**, [Al(OC$_{10}$F$_{15}$)$_4$]$^-$), −121.7 (m, C**F$_2$**, [Al(OC$_{10}$F$_{15}$)$_4$]$^-$) ppm.

^{27}Al-NMR (78.22 MHz, 298 K, THF/CDCl$_3$): δ = 34.2 (s, 1Al, [**Al**(OC$_{10}$F$_{15}$)$_4$]$^-$) ppm.
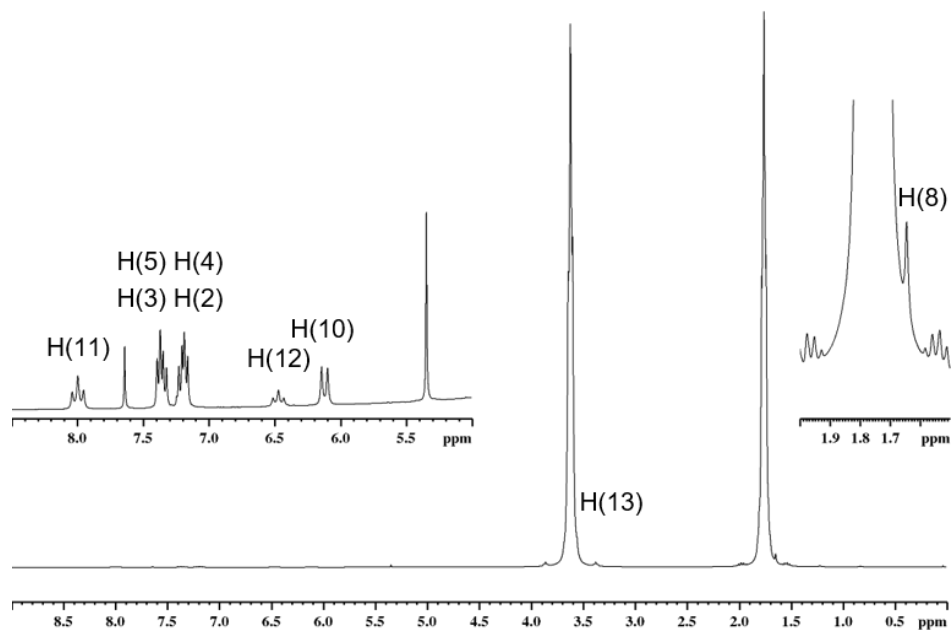
Figure S1.9. ^{1}H-NMR spectrum (300.18 MHz, 298 K, THF/CDCl$_3$) Synthesis of [Cy5][Al(pfad)$_4$] by reaction of Li[Al(pfad)$_4$] with [Cy5][BF$_4$] in CH$_2$Cl$_2$ after crystallization with n-pentane, calibrated on THF.
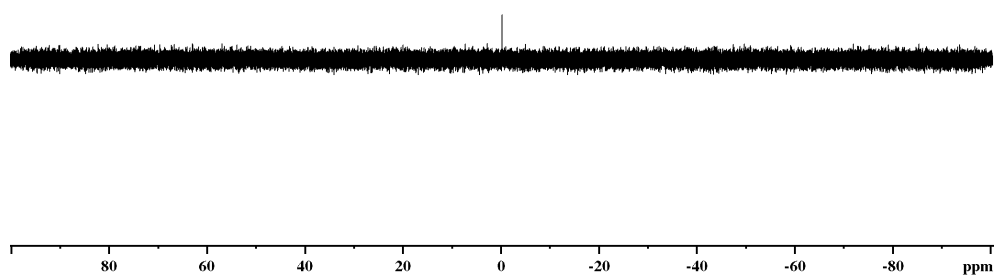
Figure S1.10. ^{7}Li-NMR spectrum (116.66 MHz, 298 K, THF/CDCl$_3$) Synthesis of [Cy5][Al(pfad)$_4$] by reaction of Li[Al(pfad)$_4$] with [Cy5][BF$_4$] in CH$_2$Cl$_2$ after crystallization with n-pentane, calibrated on THF. => Li$^+$ is absent.

9
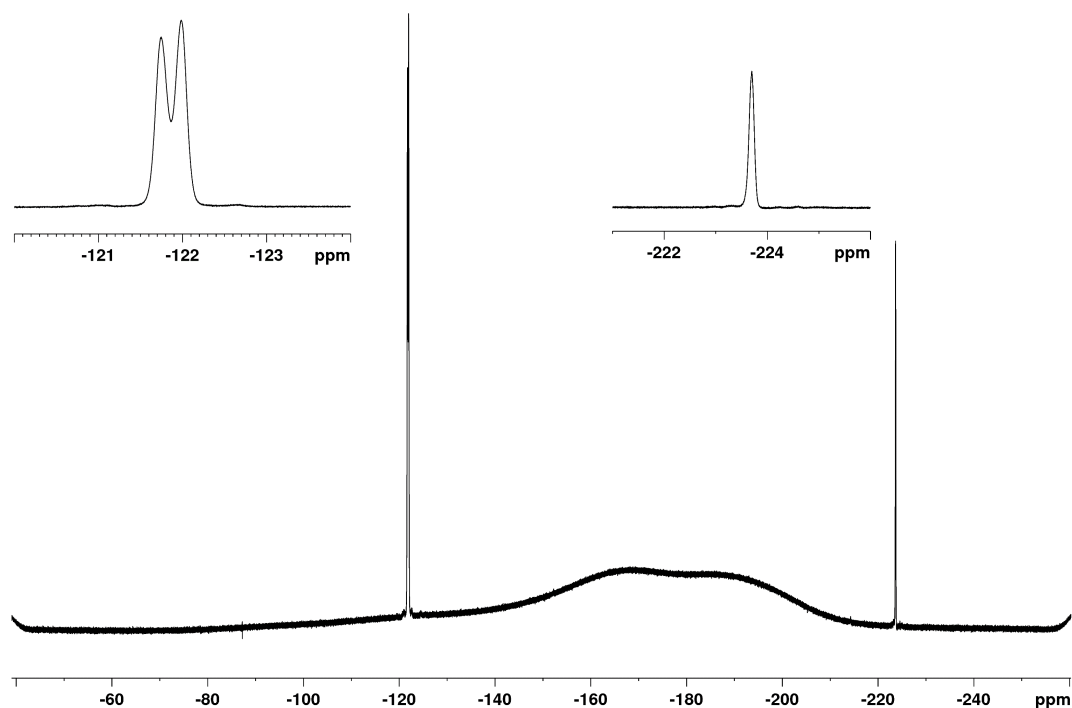
Figure S1.11. ^{19}F-NMR spectrum (282.45 MHz, 298 K, THF/CDCl$_3$) Synthesis of [Cy5][Al(pfad)$_4$] by reaction of Li[Al(pfad)$_4$] with [Cy5][BF$_4$] in CH$_2$Cl$_2$ after crystallization with n-pentane, calibrated on THF.
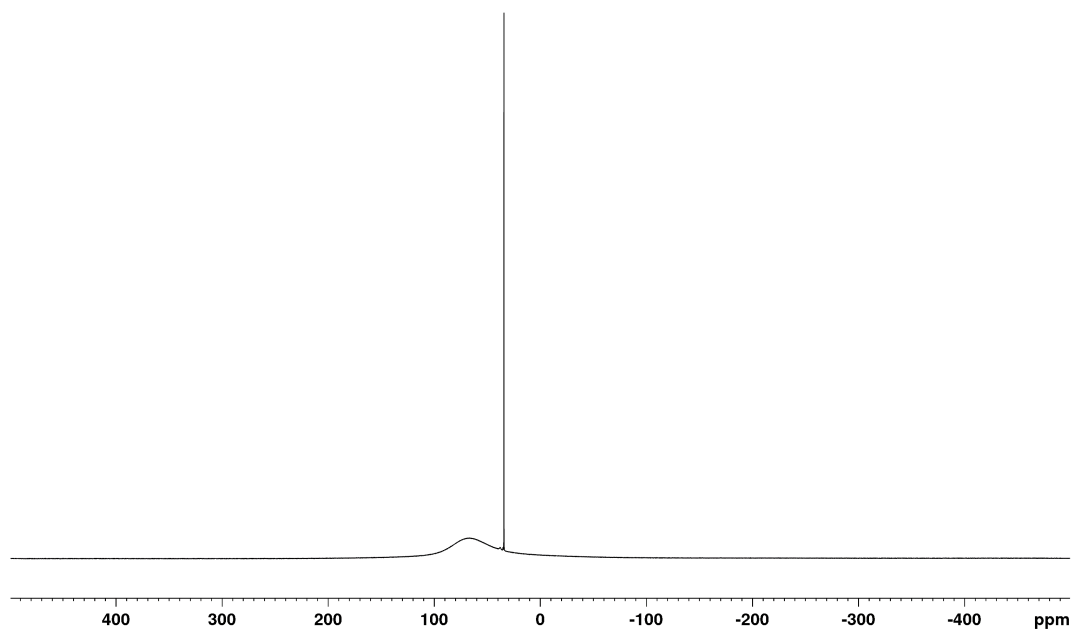
Figure S1.12. ^{27}Al-NMR spectrum (78.22 MHz, 298 K, THF/CDCl$_3$) Synthesis of [Cy5][Al(pfad)$_4$] by reaction of Li[Al(pfad)$_4$] with [Cy5][BF$_4$] in CH$_2$Cl$_2$ after crystallization with n-pentane, calibrated on THF.

S2. Ultrafast transient absorption dynamics and the global fitting procedure
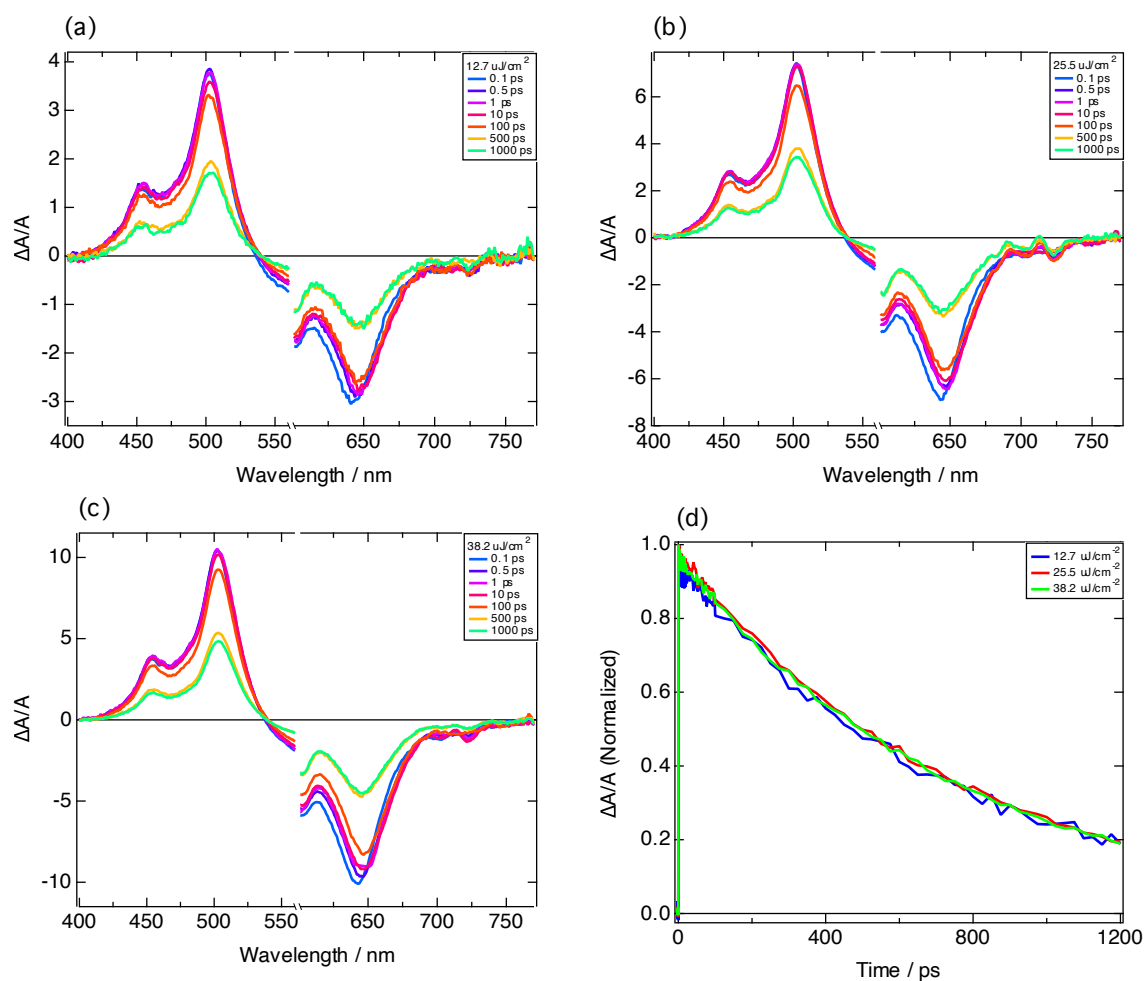
Figure S2.1. Transient absorption spectra of Cy5-P in solution at different fluences: (a) 12.7 μJcm^{-2}, (b) 25.5 μJcm^{-2} and (c) 38.8 μJcm^{-2}. Figure (d) shows the fluence independence kinetics of the feature at 502 nm.
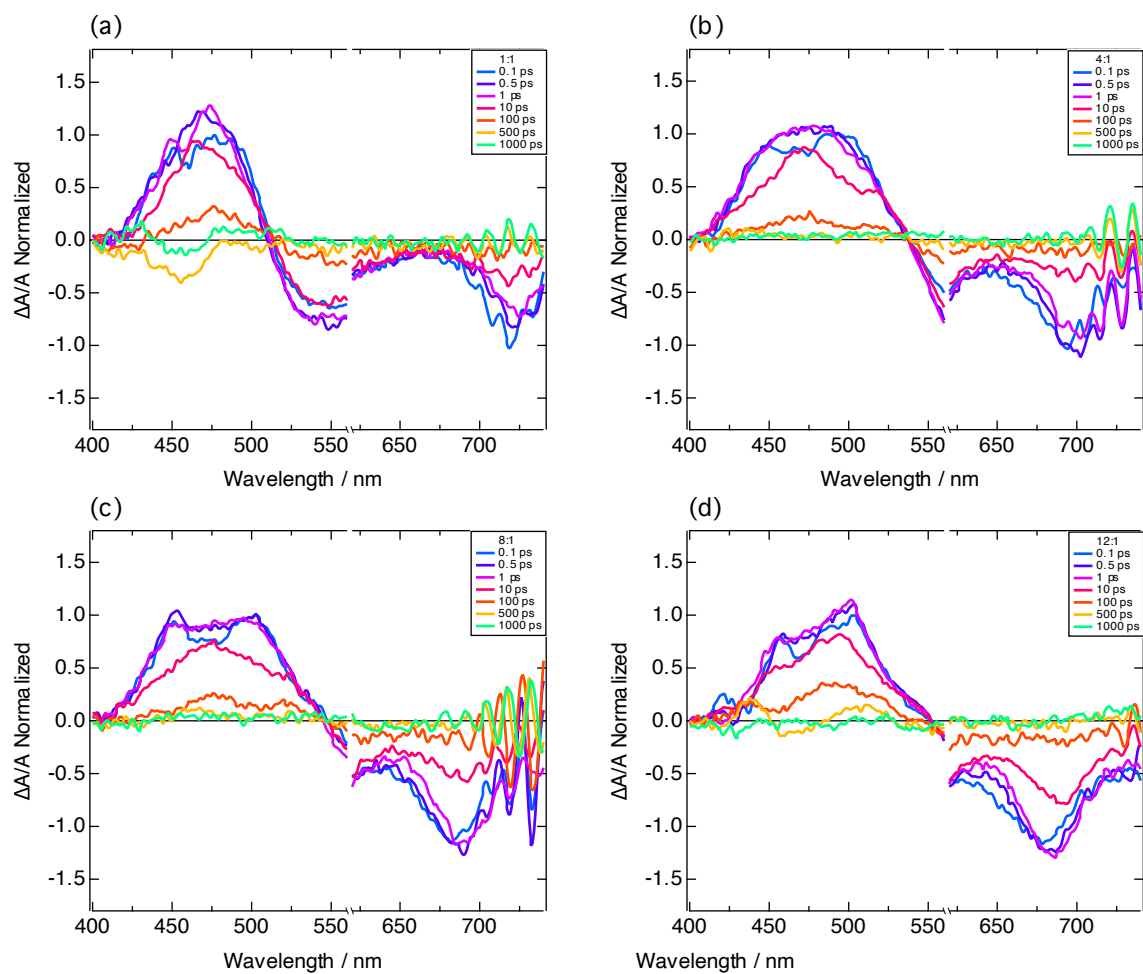
Figure S2.2. Transient absorption spectra of different PMMA:Cy5-P blends: (a) 1:1, (b) 4:1, (c) 8:1 and (d) 12:1. The spectra have been normalised to the signal at 100 fs for ease of comparison between the different blends.

Fitting of kinetic equations

The dynamic traces obtained from fs-transient absorption measurements were fitted with the following multi-exponential functions:

    a) Bi-exponential function:

$$\Delta A(\lambda, t) = A_0 + A_1(\lambda) \cdot \exp\left(\frac{-t}{\tau_1}\right) + A_2(\lambda) \cdot \exp\left(\frac{-t}{\tau_2}\right)$$

    b) Tri-exponential function:

$$\Delta A(\lambda, t) = A_0 + A_1(\lambda) \cdot \exp\left(\frac{-t}{\tau_1}\right) + A_2(\lambda) \cdot \exp\left(\frac{-t}{\tau_2}\right) + A_3(\lambda) \cdot \exp\left(\frac{-t}{\tau_3}\right)$$

Global Fitting Procedure [7-9]

Global fitting was used on our data in order to help elucidate the charge transfer processes taking place within the Cy5 thin films, as well as to calculate the quantum yield of charge separation (see S5 for more details). A more comprehensive review of global analysis can be found in the following literature.[10, 11]

To perform a global fit, the data must first be sampled and an appropriate number of kinetic traces should be extracted; this allows for a suitable fit (and subsequent decay associated spectra) to be achieved, whilst minimising the amount of time required for the fit. Once sampled, a kinetic model is applied (here either a bi- or tri-exponential function) whereby all of the traces are forced to evolve with the same time constant(s). The following step-by-step procedure was used to obtain the global fits along with the use of Igor Pro (WaveMetrics) global fit software package.

1) Extract kinetics traces every 5 nm between 400 nm and 760 nm (excluding 560-620 nm due to λ_{ex} being 580 nm).
2) Manually fit a few of the extracted kinetic traces in order to obtain an accurate fitting equation and to provide a reasonable first guess for the global fit.
3) Select the appropriate fitting function from step 2. Link the time constant(s) for the kinetic traces, and provide initial values for the fitting coefficients based on the guesses found in step 2.
4) Perform the global fit with a suitable number of iterations (typically 40). If convergence is reached, assess the quality of the fit by examining the calculated residuals. If the fit does not converge, the initial guesses should be changed and the process repeated.
5) The amplitude coefficient(s) can subsequently be extracted into new sets of data, which can then be plotted against the wavelengths used in the global fit to give the decay associated spectra.
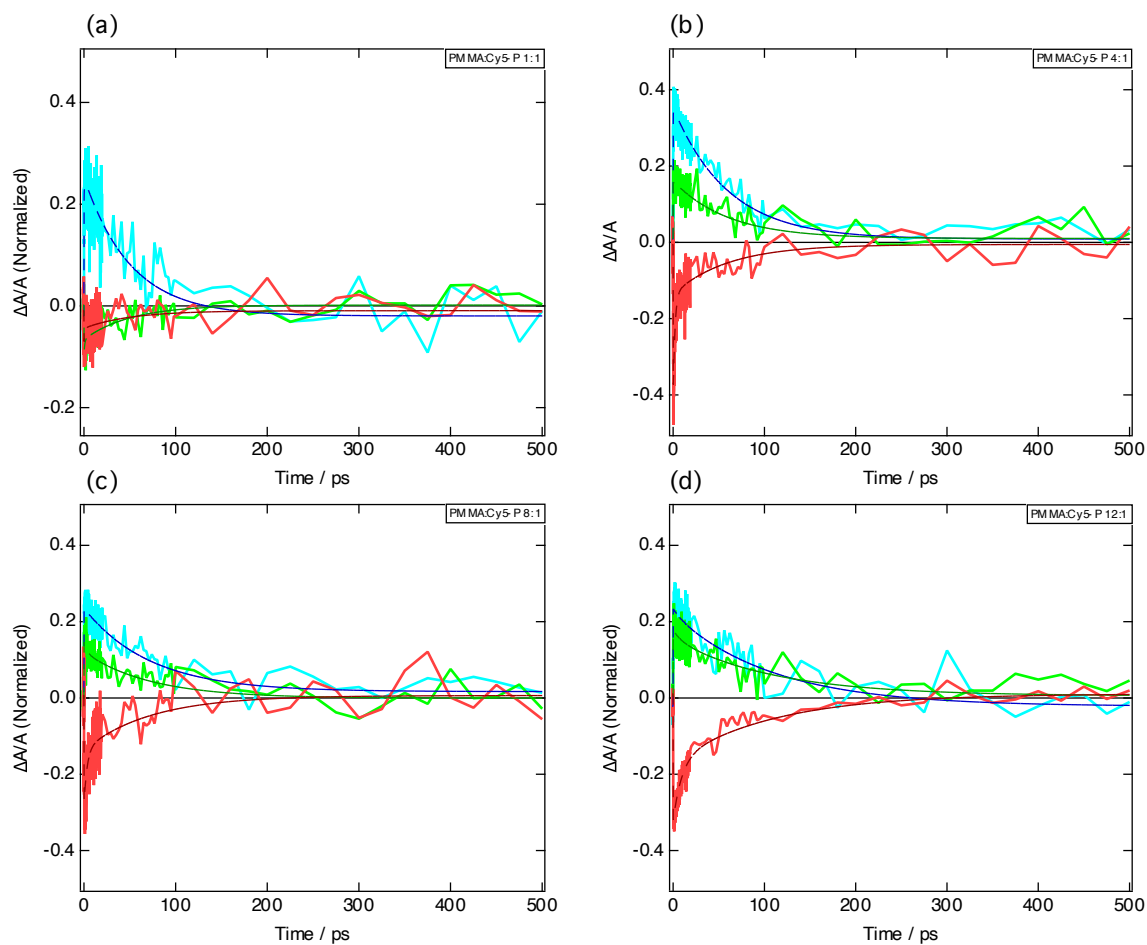
Figure S2.3. Kinetic traces at 470 (blue), 520 (green) and 700 nm (red) for different ratios of PMMA:Cy5-P thin films. The dashed lines show the results of the global fitting procedure.
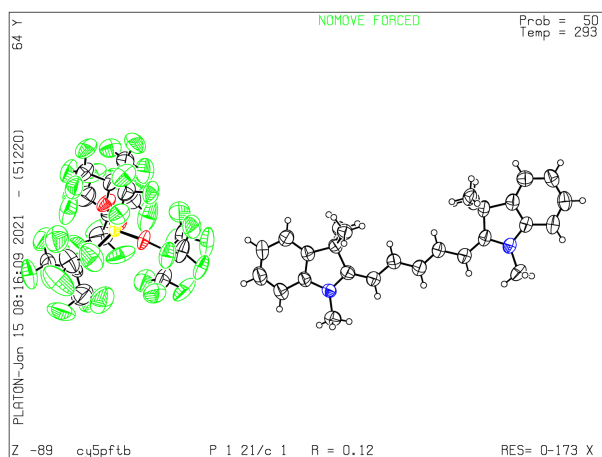
Table S2. Results from global fits of TA spectra of different molar ratios of PMMA:Cy5-P blends, fitted with biexponential functions.

PMMA:Cy5-P Blend ratio	τ_1 / ps	τ_2 / ps
1:1	0.85	47
4:1	2.0	62
8:1	3.4	75
12:1	8.4	103

S3. SC-XRD details and summary of Hirshfeld surface analysis [12, 13]

Structure Tables

	Cy5-[Al(pftb)$_4$]	Cy5-[Al(pfad)$_4$]	Cy5-PF$_6$
CCDC number		2056417	2044614
Empirical formula	C$_{172}$H$_{124}$Al$_4$F$_{144}$N$_8$O$_{16}$	C$_{68}$H$_{33}$AlCl$_2$F$_{60}$N$_2$O$_4$	C$_{27}$H$_{31}$F$_6$N$_2$P
Formula weight	5402.70	2178.30	528.51
Temperature [K]	293(2)	100(2)	100(2)
Crystal system	monoclinic	triclinic	monoclinic
Space group (number)	$P2_1/c$ (14)	$P\overline{1}$ (2)	$P2_1/c$ (14)
a [Å]	11.4785(10)	12.925(3)	12.4822(9)
b [Å]	27.720(3)	13.451(3)	18.8248(12)
c [Å]	16.5740(16)	22.359(3)	12.0756(8)
α [°]	90	90.353(3)	90
β [°]	92.346(7)	92.653(4)	118.153(2)
γ [°]	90	93.709(4)	90
Volume [Å^3]	5269.2(9)	3874.7(12)	2501.8(3)
Z	1	2	4
ρ_{calc} [g/cm^3]	1.703	1.867	1.403
μ [mm^{-1}]	0.210	0.291	0.174
F(000)	2688	2145	1104
Crystal size [mm^3]	0.15×0.12×0.10	0.27×0.21×0.15	0.200×0.050×0.050
Crystal colour	blue	black	blue
Crystal shape	block	plate	needle
Radiation	MoK_α (λ=0.71073 Å)	MoK_α (λ=0.71073 Å)	MoK_α (λ=0.71073 Å)
2Θ range [°]	2.86 to 50.65 (0.83 Å)	1.82 to 55.87 (0.76 Å)	3.70 to 56.63 (0.75 Å)
Index ranges	-13 ≤ h ≤ 12	≤ h ≤	-16 ≤ h ≤ 16
	-33 ≤ k ≤ 32	≤ k ≤	-25 ≤ k ≤ 25
	-19 ≤ l ≤ 19	≤ l ≤	-16 ≤ l ≤ 16
Reflections collected	34148	17443	63205
Independent reflections	9269	17443	6174
	R_{int} = 0.1611	R_{int} = 0.0378	R_{int} = 0.0589
	R_{sigma} = 0.1279	R_{sigma} = 0.0505	R_{sigma} = 0.0331
Completeness	97.2 %	96.4 %	100.0 %
Data / Restraints / Parameters	9269/388/781	17443/18373/1968	6174/0/332
Goodness-of-fit on F^2	1.016	1.156	1.017
Final R indexes [$I\geq2\sigma(I)$]	R_1 = 0.1165 / wR_2 = 0.3021	R_1 = 0.0554 / wR_2 = 0.1595	R_1 = 0.0478 / wR_2 = 0.1199
Final R indexes [all data]	R_1 = 0.2059 / wR_2 = 0.3633	R_1 = 0.0886 / wR_2 = 0.1725	R_1 = 0.0690 / wR_2 = 0.1344
Largest peak/hole [eÅ^3]	1.33/-0.60	0.93/-0.50	0.56/-0.42
Extinction coefficient	—	—	0.0039(7)

Molecular structure of Cy5-[Al(pftb)$_4$]
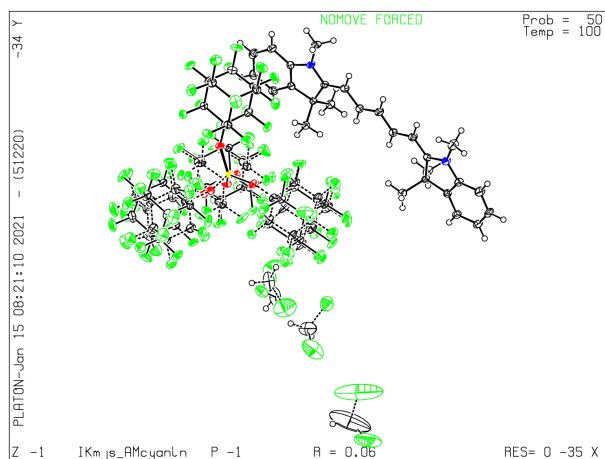
Molecular structure of Cy5-[Al(pfad)$_4$]
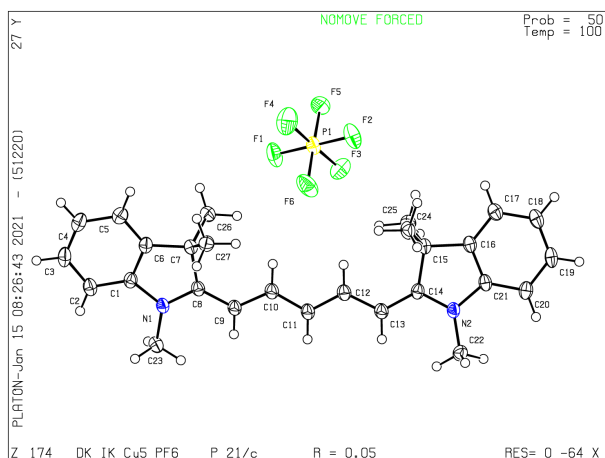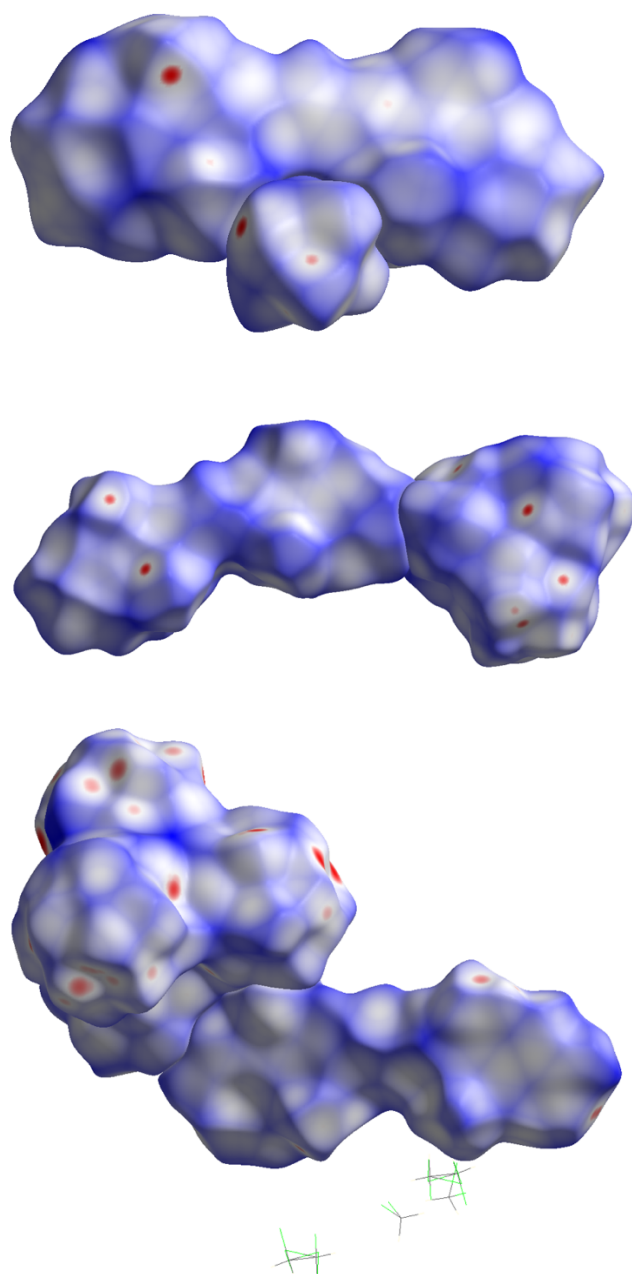

Molecular structure of Cy5-PF$_6$

16

Figure S3.1. Hirshfeld surfaces of Cy5-PF$_6$ (top), Cy5-[Al(pftb)$_4$] (middle) and Cy5-[Al(pfad)$_4$] (bottom)

Table S3.1. Relative contributions to the Hirshfeld surface area for the intermolecular contacts in Cy5-PF6, Cy5-[Al(pftb)$_4$] and Cy5-[Al(pfad)$_4$] in percent.

	Cation					Anion		
	H...H	C...H	C...C	N...all	H...F	F...H	F...C	F...F
Cy5-PF$_6$	21.7	23.4	0.6	1.2	21.7	97.2	0.6	1.3
Cy5-[Al(pftb)$_4$]	25.6	12.7	1.0	1.0	54.3	62.2	4.0	33.5
Cy5-[Al(pfad)$_4$]	13.6	9.7	0.8	1.2	61.8	49.4	2.9	44.2

Table S3.2. Cation-Cation contacts in percent and Volume ratio of cation to anion in Cy5-PF$_6$, Cy5-[Al(pftb)$_4$] and Cy5-[Al(pfad)$_4$].

	∑Cat...Cat contacts [%]	V(C+)/V(A−)
Cy5-Cl		~18 [a)]
Cy5- PF$_6$	76.8	5.6
Cy5-[Al(pftb)$_4$]	40.5	0.8
Cy5-[Al(pfad)$_4$]	25.4	0.5

[a)] Estimated value based on V(C+) of Cy5-PF$_6$ and V(A−) of CCDC structure DODQUK.

For the cations, H-H contacts dominate for Cy5-[Al(pftb)$_4$] and Cy5-[Al(pfad)$_4$], but C-H contacts dominate for Cy5-PF$_6$. The clear difference is even more pronounced in the H-F contacts where Cy5-[Al(pftb)$_4$] has twice as many contacts as Cy5-PF$_6$ and Cy5-[Al(pfad)$_4$] even three times more. C-C and N-all contacts only play a minor role around one percent.

With the anions, there is also a clear difference for the smaller PF$_6^-$ and the other two anions. In Cy5-PF$_6$, nearly all contacts of the anion go to hydrogen atoms of the cation. But for Cy5-[Al(pftb)$_4$] and Cy5-[Al(pfad)$_4$], only 62% and 50% of the contacts are to the cation respectively. The two larger anions have more F-F contacts to other anions while PF$_6^-$ has nearly no contacts to other anions.

Cy5-[Al(pfad)$_4$]
Cation-Cation contacts: 0.8(CC)+9.7(CH)+0.9(CN)+13.6(HH)+0.4(HN) = 25,4%
Cell volume: 3874.7 Å^3
Cy5-Cation Hirshfeld volume = 573,29 Å^3
Al(pfad)$_4$ - Anion = 1194.08 Å^3

Cy5-[Al(pftb)$_4$]
Cation-Cation contacts: 1.0(CC)+ 12.7(CH)+ 1.0(CN)+ 25.6(HH)+ 0.2(HN) = 40.5%
Cell volume: 5269.10 Å^3
Cy5-Cation Hirshfeld volume = 595.12 Å^3
Al(pftb)$_4$ - Anion = 707.49 Å^3

Cy5-PF$_6$

Cation-Cation contacts: 0.6(CC)+0.4(NC)+0.7(NH)+23.4(CH)+51.7(HH) = 76.8%

Cell volume: 2501.8 Å^3

Cy5-Cation Hirshfeld. volume = 520,87 Å^3

PF$_6$ - Anion = 92.91 Å^3
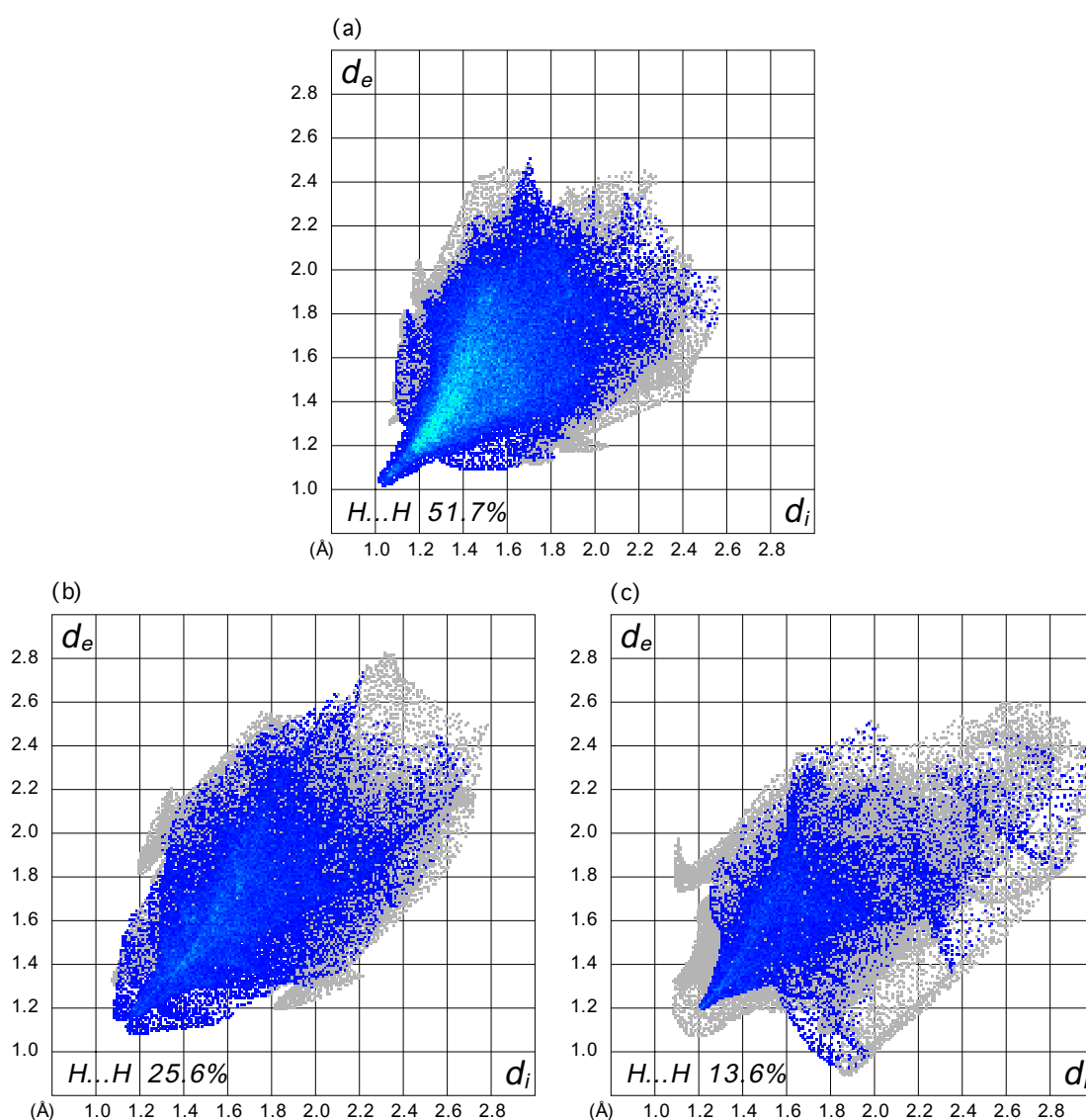
Cl$^-$

Volume of Cl$^-$: ~29 Å^3

Figure S3.2. Fingerprint plots showing the distribution of inter-cationic H-H contacts for (a) Cy5-PF$_6$, (b) Cy5-[Al(pftb)$_4$] and (c) Cy5-[(pfad)$_4$].
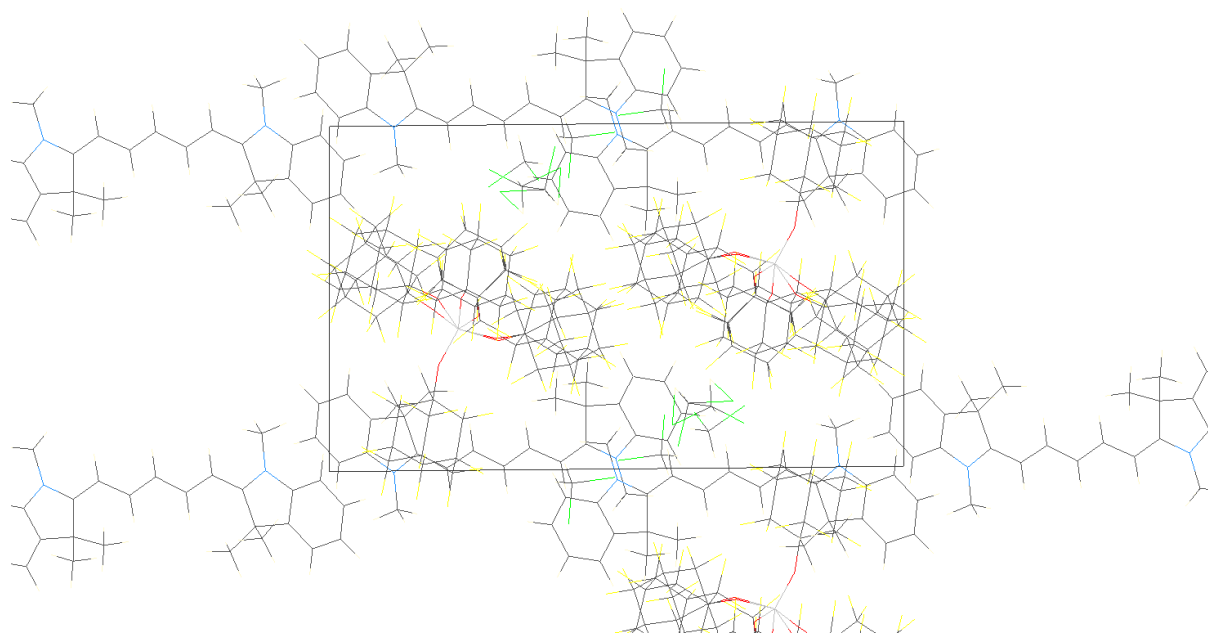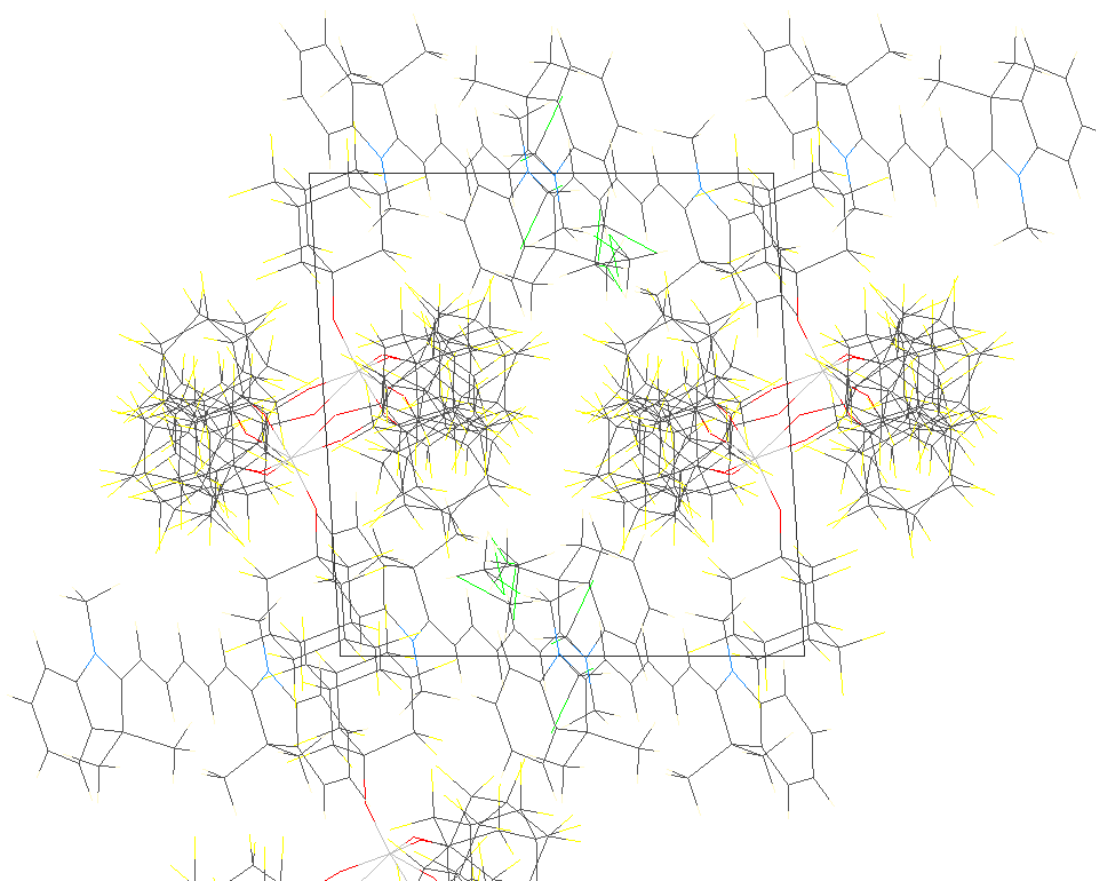
Figure S3.3. Packing of Cy5-[Al(pfad)$_4$] along a-axis.

Figure S3.4. Packing of Cy5-[Al(pfad)$_4$] along c-axis.
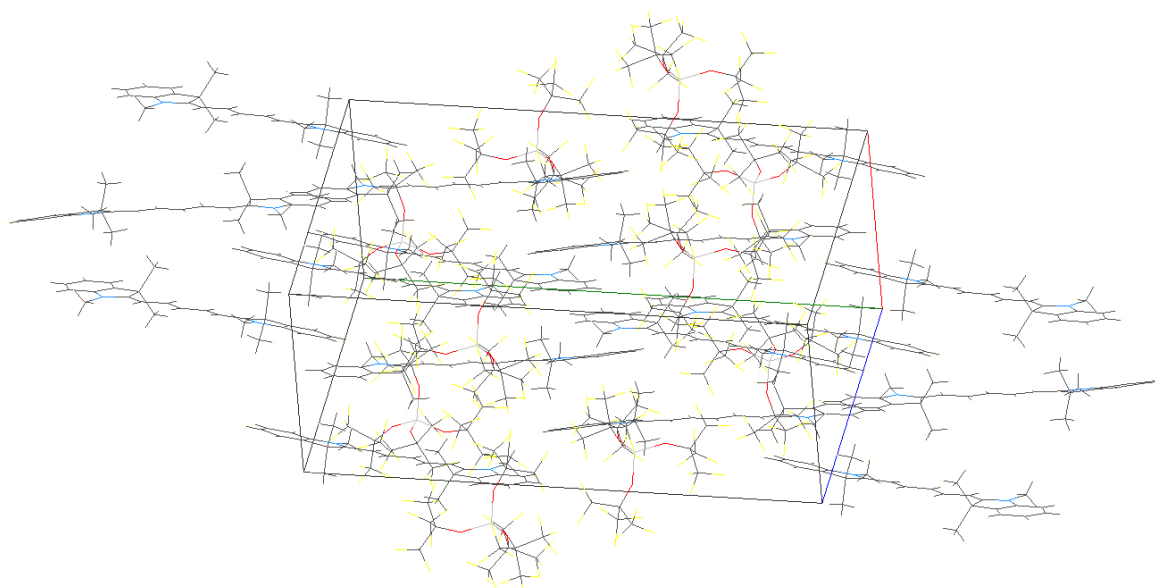
Figure S3.5. Packing of Cy5-[Al(pftb)$_4$].
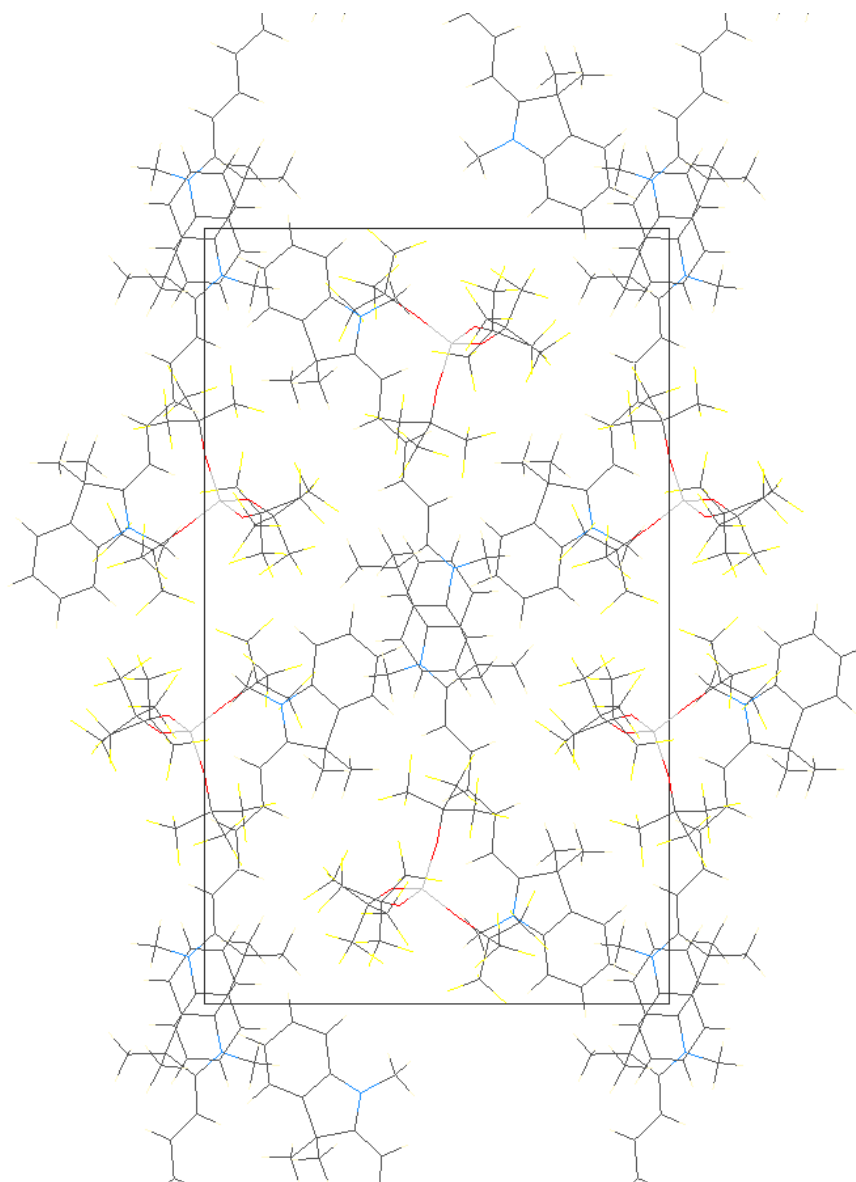
Figure S3.6. Packing of Cy5-[Al(pftb)₄] along a-axis.
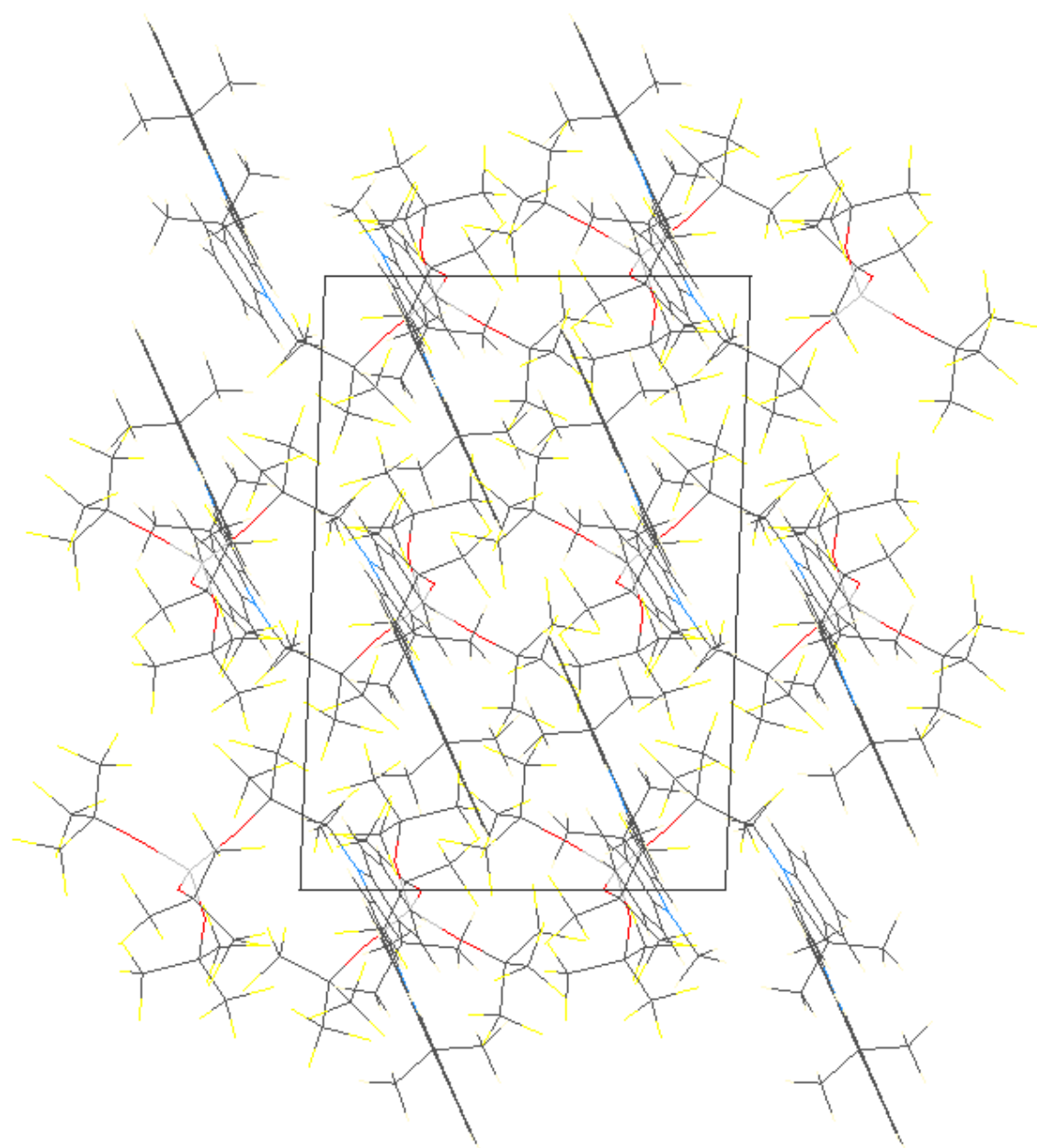
Figure S3.7. Packing of Cy5-[Al(pftb)₄] along b-axis.
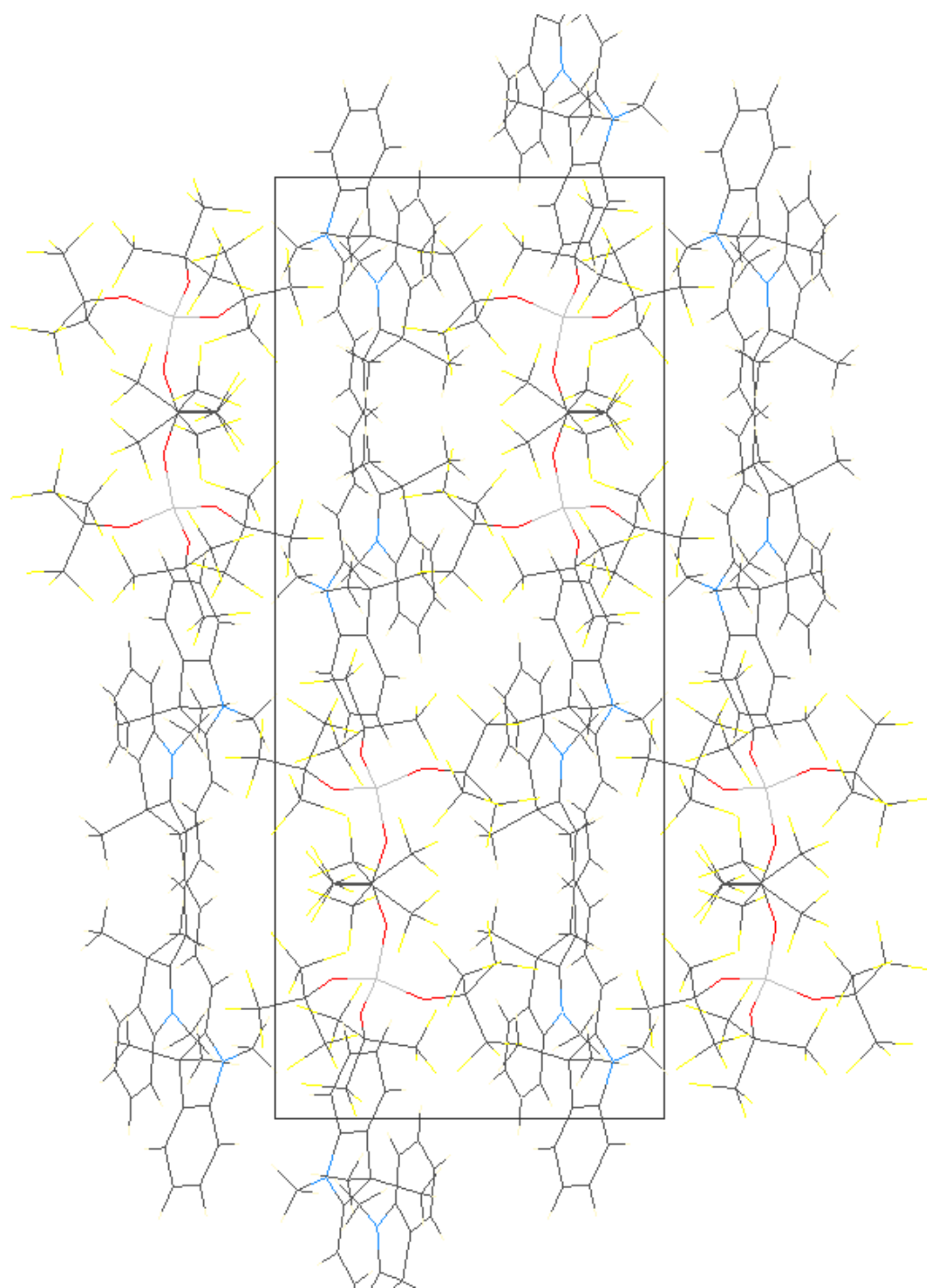
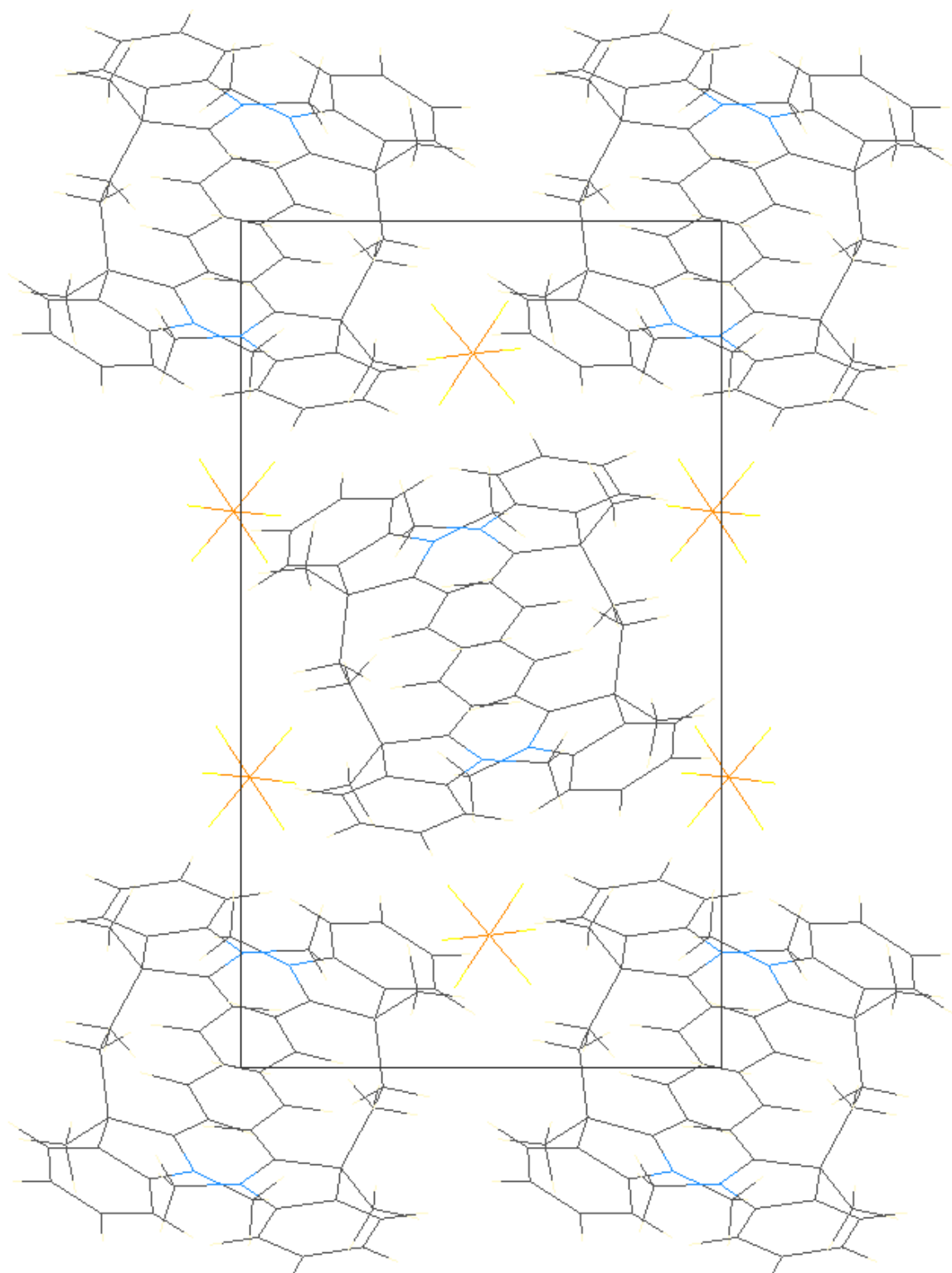**Figure S3.8.** Packing of Cy5-[Al(pftb)$_4$] along c-axis.
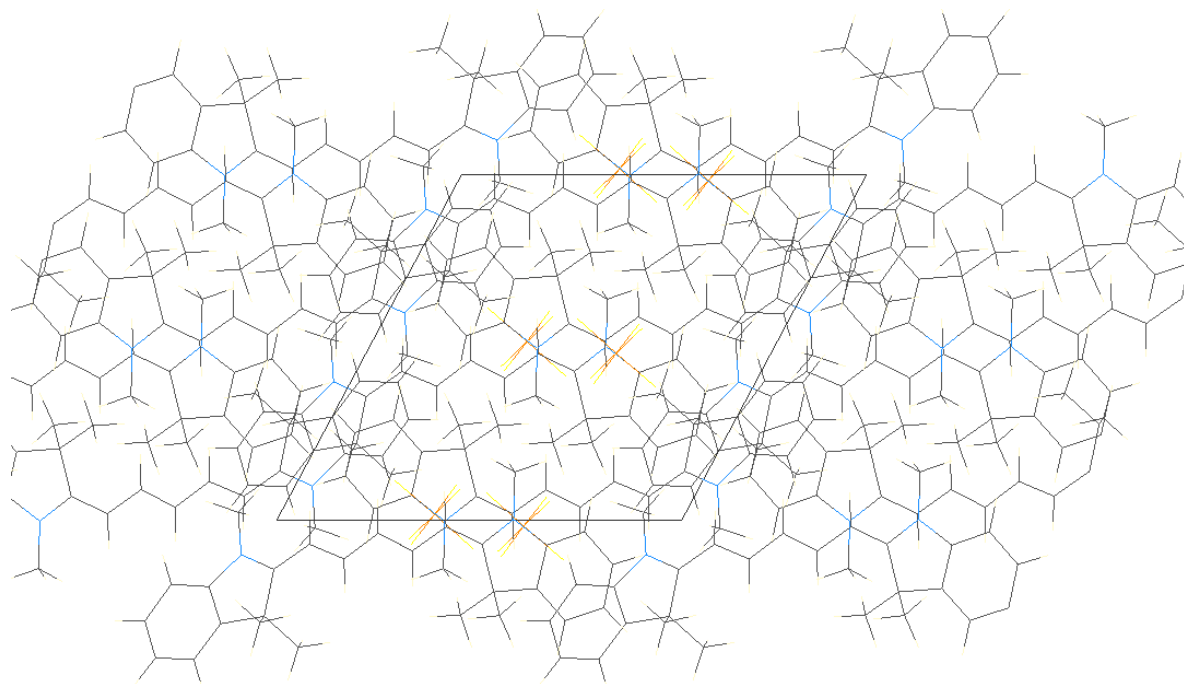
Figure S3.9. Packing of Cy5-PF$_6$.

Figure S3.10. Packing of Cy5-PF$_6$ along a-axis.

Figure S3.11. Packing of Cy5-PF$_6$ along b-axis
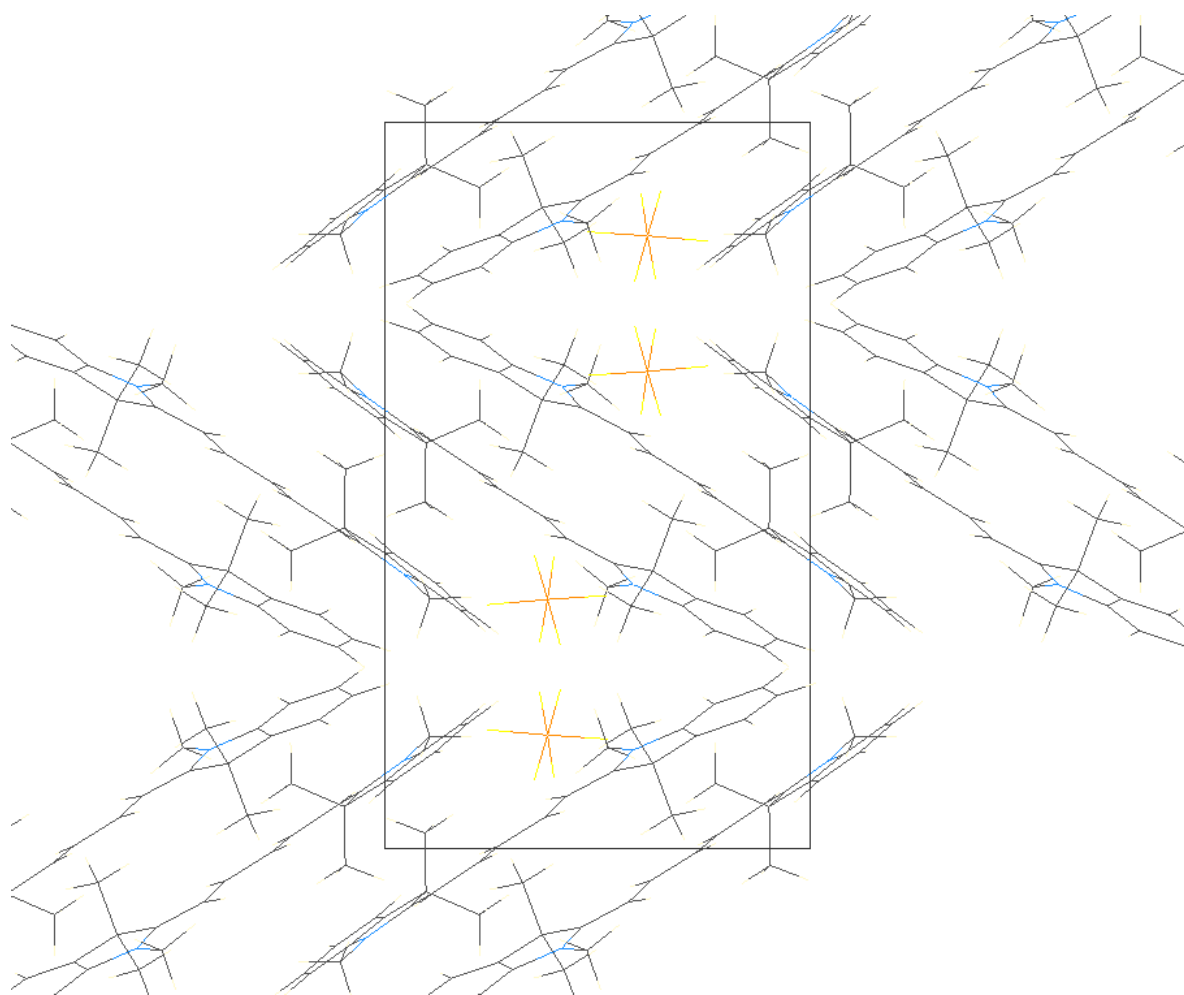
Figure S3.12. Packing of Cy5-PF$_6$ along c-axis.
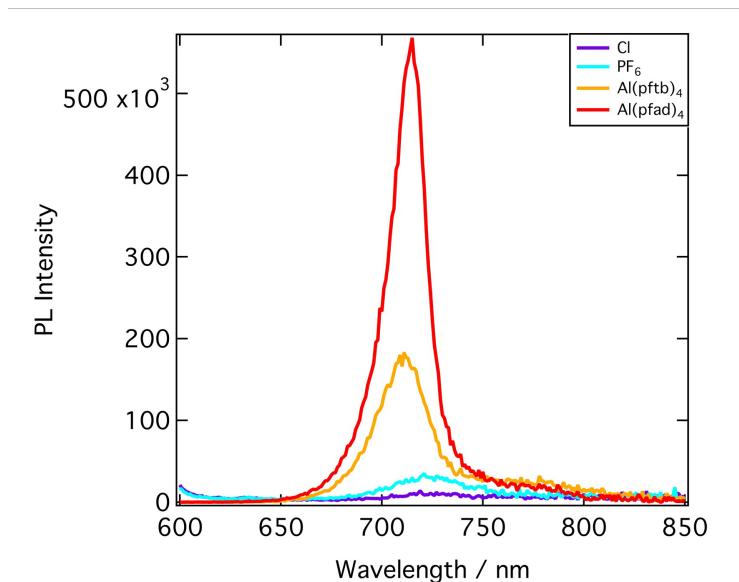
S4. Optical characterization and global fits

Figure S4.1. Steady state emission for different Cy5 thin films: Cl (purple), PF$_6$ (cyano), [Al(pftb)$_4$] (orange) and [Al(pfad)$_4$] (red).
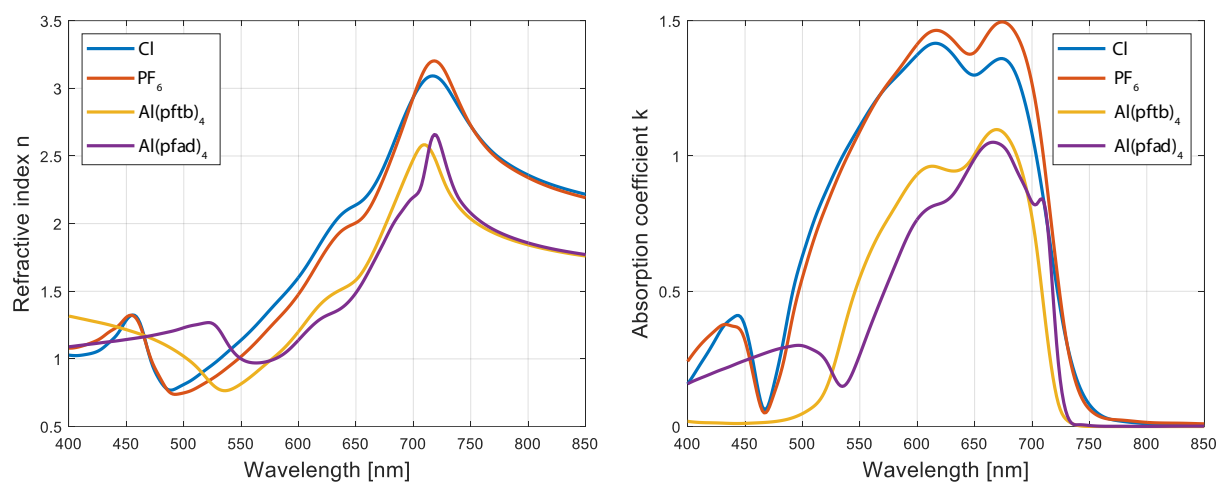

Figure S4.2. Optical constants *n* and *k* as measured by ellipsometry.
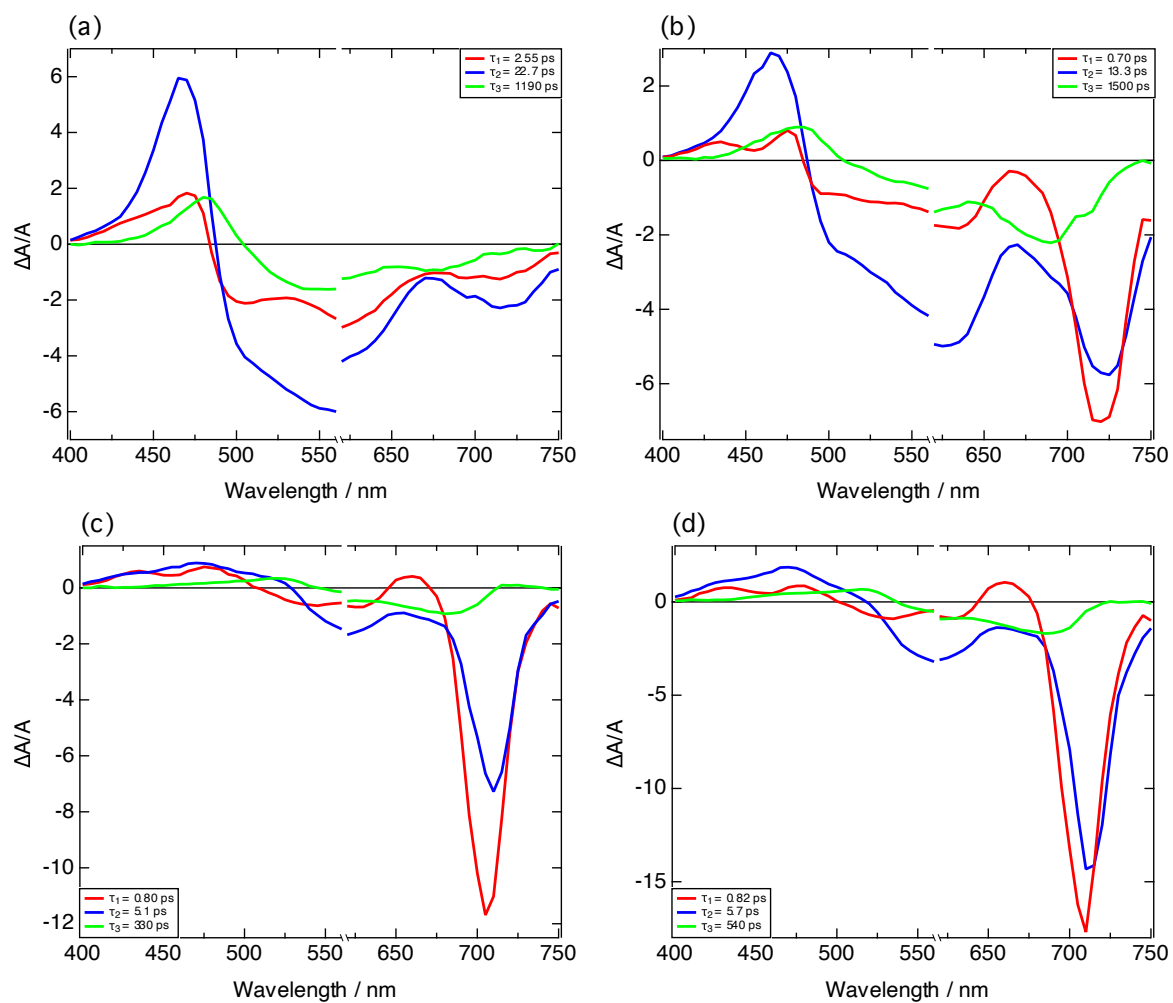
Figure S4.3. Global fits for different Cy5 thin films: (a) Cl, (b) PF$_6$, (c) [Al(pftb)$_4$] and (d) [Al(pfad)$_4$].
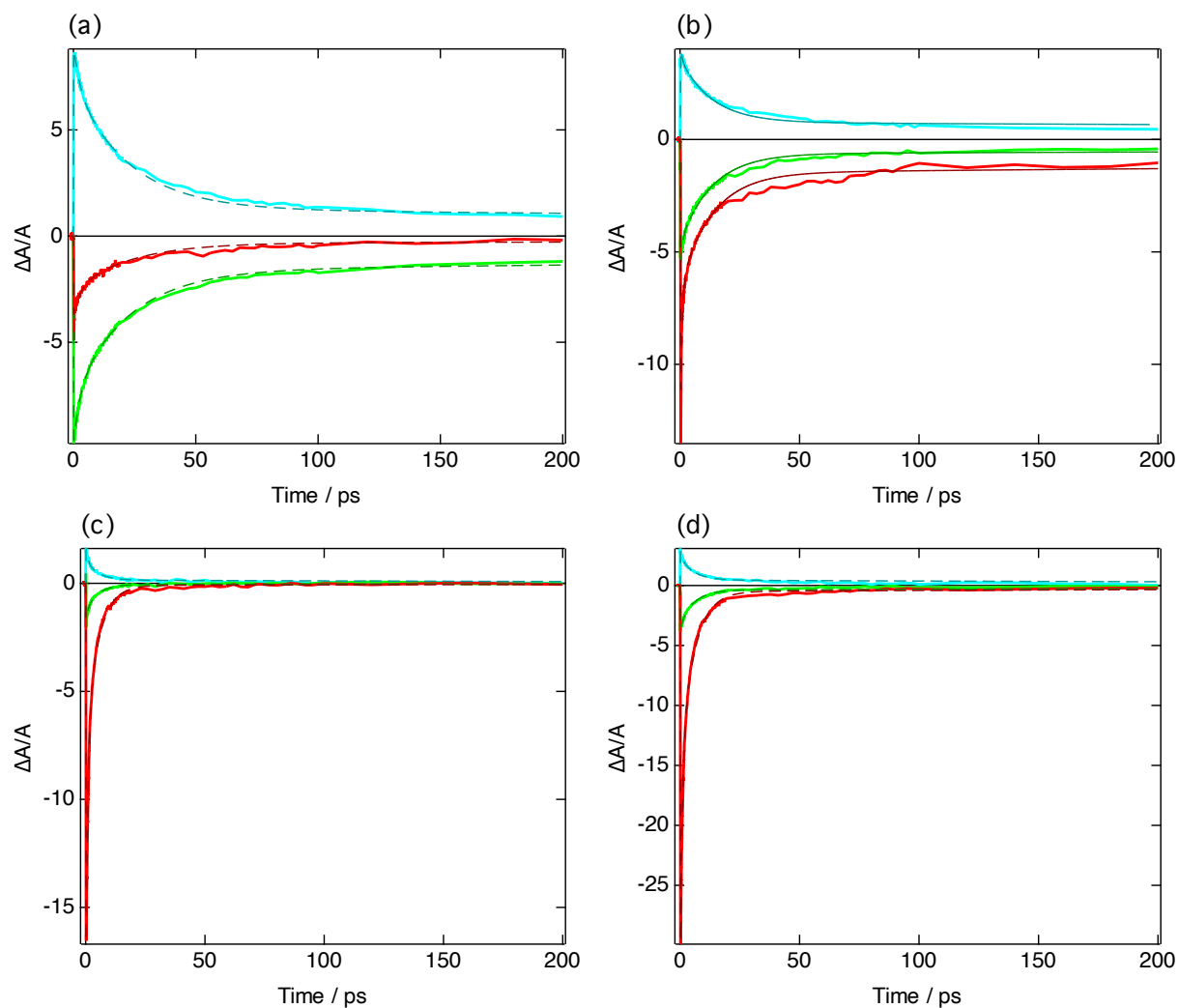
Figure S4.4. Kinetic traces at 470 (blue), 520 (green) and 700 nm (red) for Cy5-P blends incorporating different counterions: (a) Cl, (b) PF_6, (c) $[Al(pftb)_4]$ and (d) $[Al(pfad)_4]$. The dashed lines show the results of the global fitting procedure.
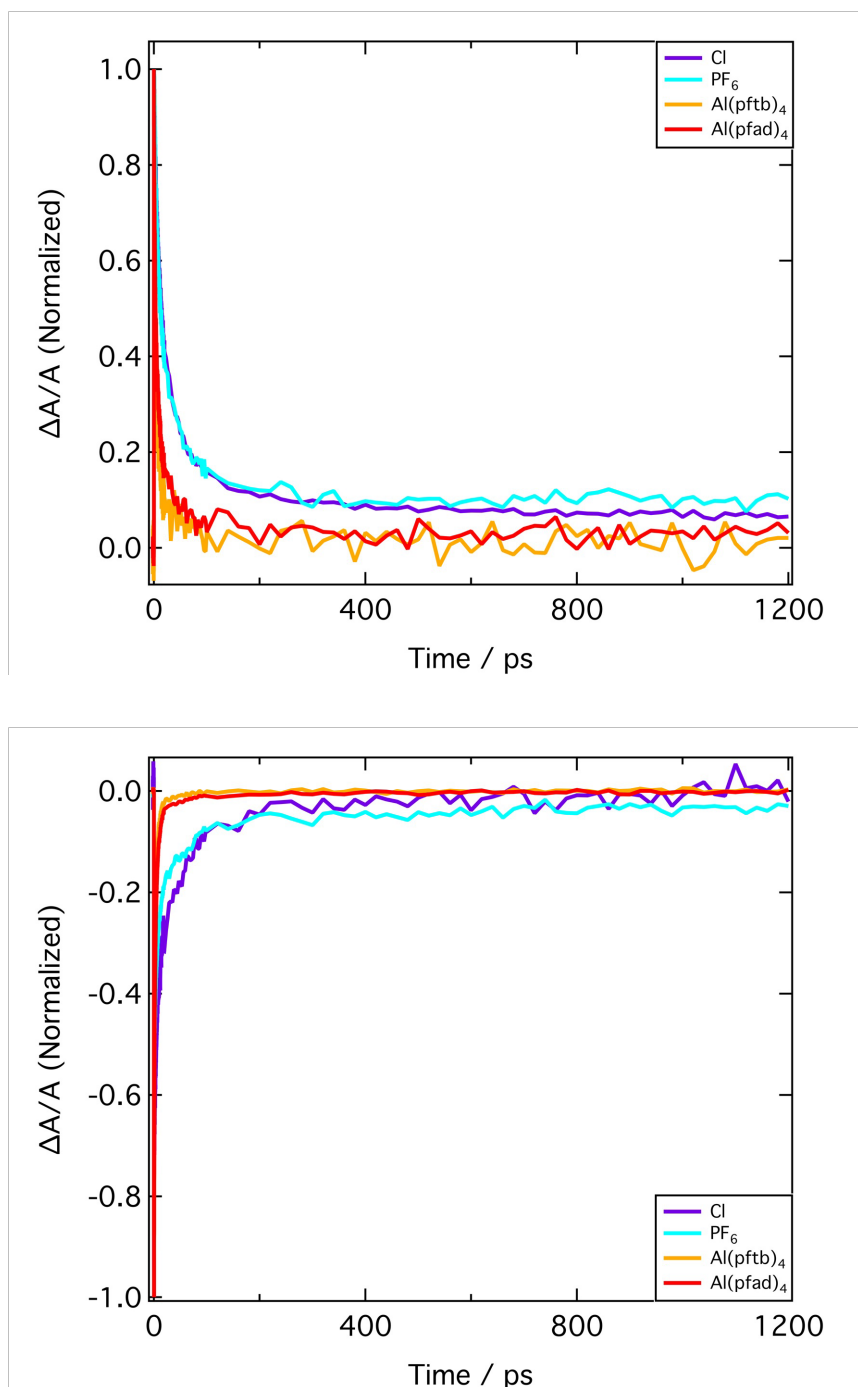
Figure S4.5. Normalized kinetic traces from TA measurements of the positive TA feature at λ = 470.5 nm (top) and the stimulated emission at λ = 710-716 nm (bottom).

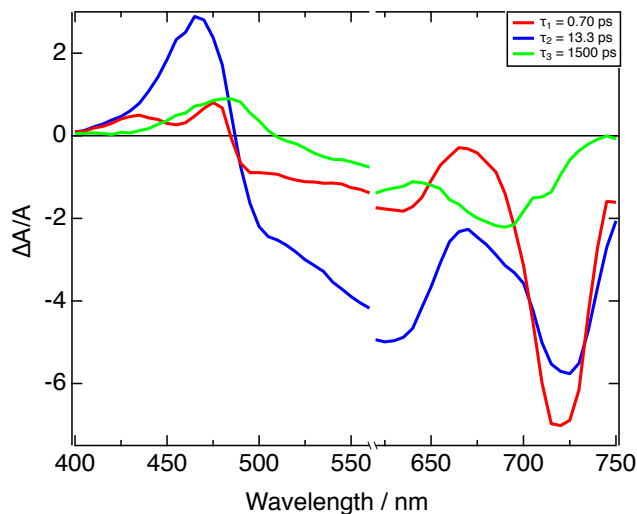## S5. Estimating the quantum yield of charge separation

Figure S5. Decay-associated difference spectra (DADS) yielded by the global fitting of the time-evolution of transient absorption spectra.

The transient spectra were fitted with a triexponential function yielding global fit plots, an example of which is shown above for the Cy5-P thin film (Fig. S3.1).

There are three components which contribute to the TA spectrum. The first component, in red, corresponds to the appearance excited state absorption, whilst the second component, in blue, corresponds to hole transfer from the aggregate excited state to a monomer in its ground state. The third component, in green, corresponds to the recombination of the separated charges.

To estimate the charge transfer yield, the area beneath the positive feature of the curve for components A_r and A_b was found and divided by the extinction coefficients of these processes. This yields the following expression:

$$Quantum\ yield\ (\%) = \frac{A_b/_{\varepsilon_{ox}}}{A_r/_{\varepsilon_{ch}} + A_b/_{\varepsilon_{ox}}}$$

Where A_r and A_b represent the area beneath the red and blue curve, and ε_{ch} and ε_{ox} are the extinction coefficients of the Cy5 chromophore and its oxidized counterpart, respectively. The extinction coefficient of the Cy5 chromophore was taken as 2.1×10^5 Lmol^{-1}cm^{-1}.

The extinction coefficient for the oxidized species was estimated from the oxidation experiments with bromine vapor, where it was found that the extinction coefficient for this process was 52 % of that of the Cy5-P dye in the ground state. Therefore, it was taken as 1.1×10^5 Lmol^{-1}cm^{-1} for the purpose of the quantum yield calculations.

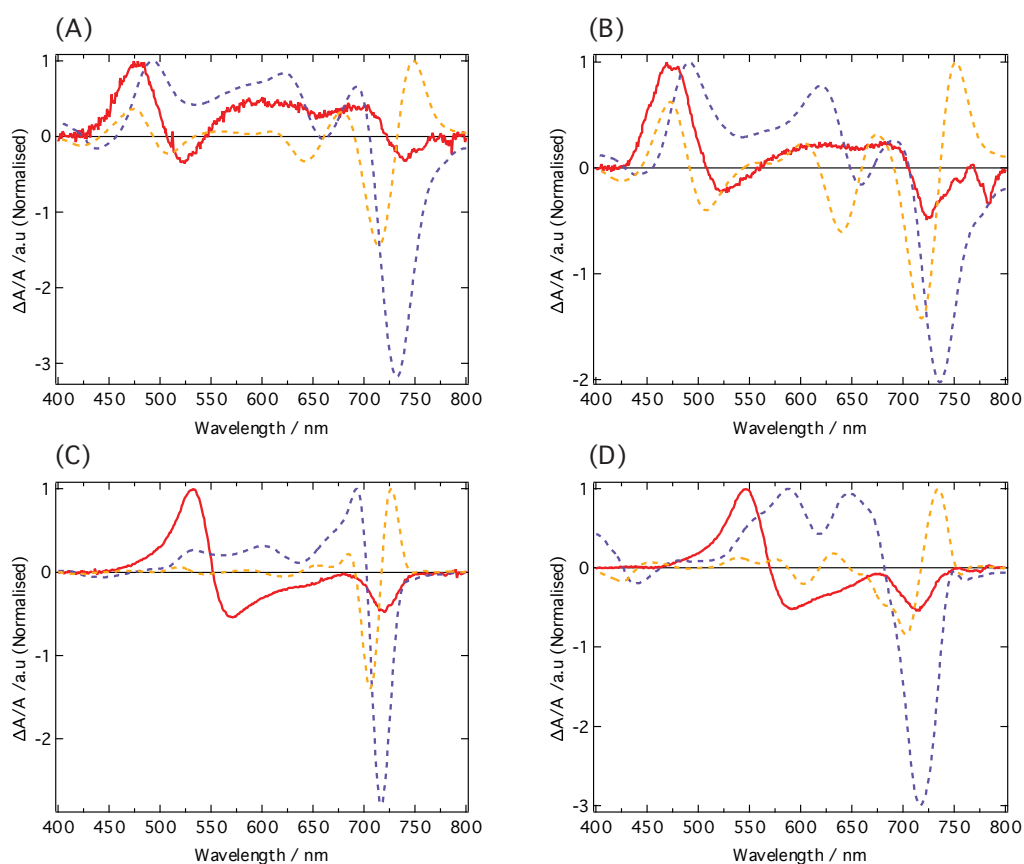## S6. Electroabsorption and time-of-flight measurements

Figure S6.1. Plots showing the normalized electroabsorption spectra (red), alongside the first and second derivatives of the absorbance spectra (dashed purple and orange lines, respectively) of Cy5 dyes with various counterions: (a) Cl$^-$, (b) PF$_6^-$, (c) [Al(pftb)$_4$]$^-$ and (d) [Al(pfad)$_4$]$^-$.
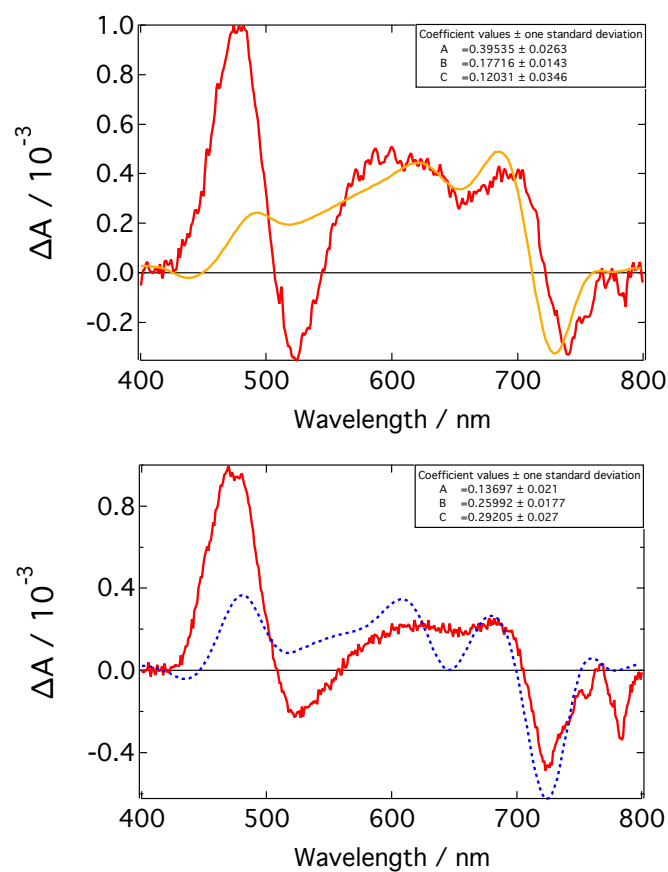
Figure S6.2. Electroabsorption spectra of Cy5-Cl (top) and Cy5-P (bottom) fitted with a linear combination of the zeroth, first and second derivatives of the steady state absorption spectra (dashed line).
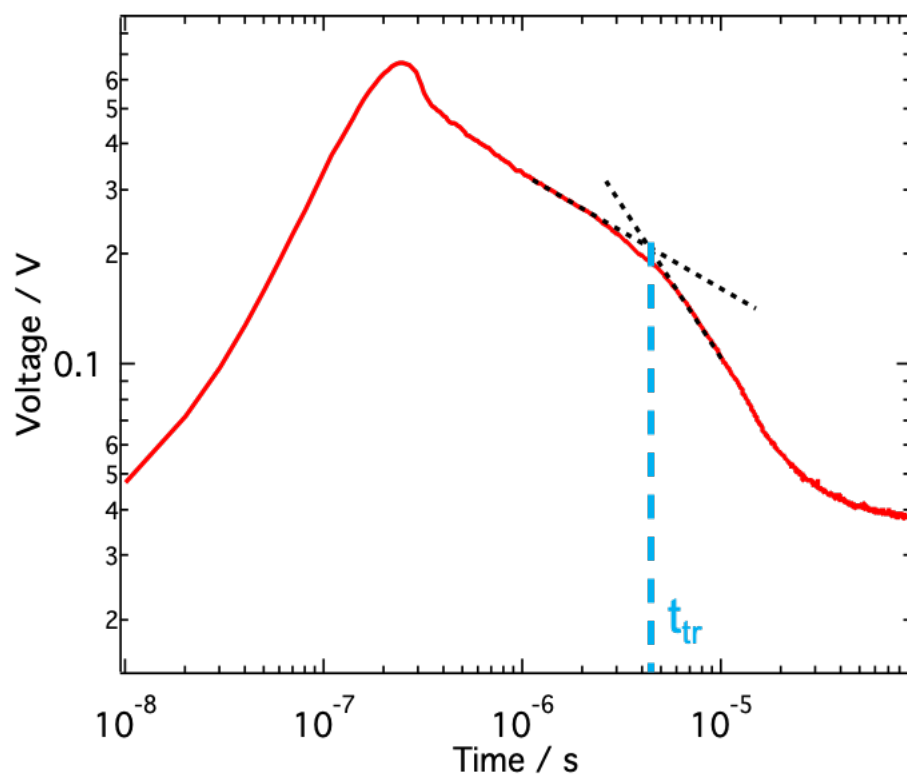
Figure S6.3. An example of a photocurrent curve from time-of-flight measurements of Cy5-P, excited at λ = 630 nm, with an applied voltage of 8 V and a resistance of 120 Ω. The transit time was found by the intersection of the two asymptotes, shown by the blue dashed line.
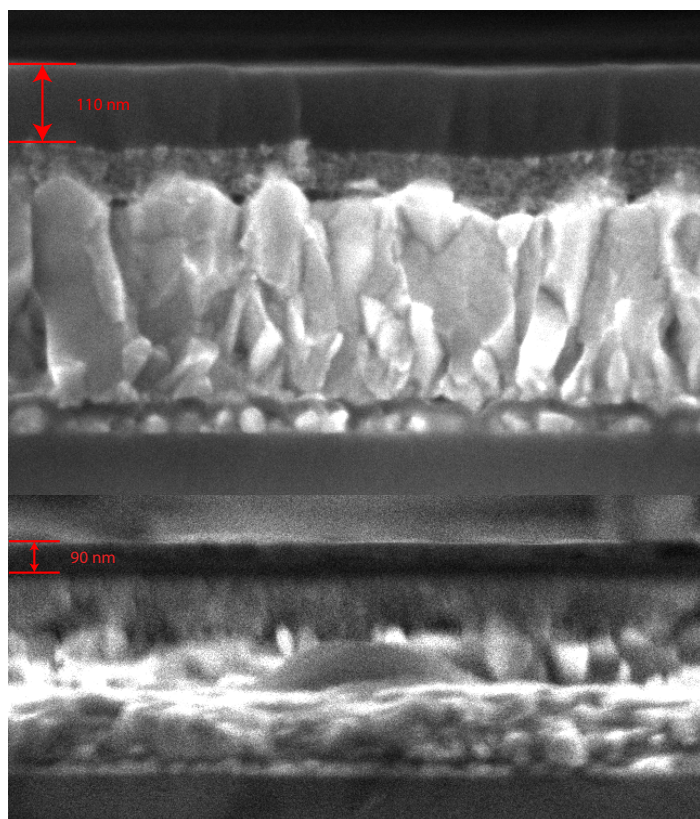
Figure S7. Cross-sectional SEM images of Cy5-Cl (top) and Cy5-P (bottom) time of flight samples. Samples had the following structure: Glass/FTO/Al$_2$O$_3$/Dye/Al. The thickness of the dye layer is shown in red.

References of SI

[1]   Bruker, *SAINT*, *V8.40B*, Bruker AXS Inc., Madison, Wisconsin, USA.

[2]   Bruker, *SADABS*, *2016/2:*, Bruker AXS Inc., Madison, Wisconsin, USA.

[3]   G. M. Sheldrick, *Acta Cryst.*, 2015, A71, 3–8.

[4]   G. M. Sheldrick, *Acta Cryst.*, 2015, C71, 3–8.

[5]   C. R. Groom, I. J. Bruno, M. P. Lightfoot and S. C. Ward, *Acta Cryst.* 2016, B72, 171–179.

[6]   D. Kratzert, *FinalCif*, V79, *https://www.xs3.uni-freiburg.de/research/finalcif*.

[7]   M. E. F. Bouduban, A. Burgos-Caminal, R. Ossola, J. Teuscher and J. E. Moser, *Chem. Sci.*, 2017, **8**, 4371-4380 (Supporting Information).

[8]   M. E. F. Bouduban, PhD thesis no. 9668, EPF Lausanne, 2019.

[9]   H.-W. Bahng, PhD thesis no. 9009, EPF Lausanne, 2019.

[10]   I. H. M. Van Stokkum, D. S. Larsen and R. Van Grondelle, *Biochim. Biophys. Acta-Bioenerg.*, 2004, **1657**, 82-104.

[11]   R. Berera, R. Van Grondelle and J. T. M. Kennis, *Photosynth. Res.*, 2009, **101**, 105-118.

[12]   N. A. Spackman and D. Jayatilaka, *CrystEngComm,* 2009, **11**, 19-32.

[13]   M. J. Turner, J. J. McKinnon, S. K. Wolff, D. J. Grimwood, P. R. Spackman, D. Jayatilaka, M. A. Spackman, *CrystalExplorer17.5*, 2017, University of Western Australia.